Heat Transfer Model Exploration in Marine Lean Burn Spark Ignition Engines

Nikolas Stylianos
Student No: 5865980

Delft University of Technology

TU Delft

Heat Transfer Model Exploration in Marine Lean Burn Spark Ignition Engines

by

Nikolas Stylianos
Student No: 5865980

Instructor:	Professor Peter de Vos
Co-Instructor:	Professor Thijs Vlugt
Teaching Assistant:	Konstantinos Kiouranakis
Faculty:	Faculty of Mechanical Engineering, Delft

TU Delft

Summary

This review examines research on marine lean burn spark ignition (SI) engines powered with natural gas (NG), focusing on a 500 kWe engine with a flat cylinder head and hemispherical bowl-in piston. These engines demonstrate cylinder flow regimes that significantly affect combustion and heat transfer. The current heat-transfer models can't capture and assess how cylinder flow regimes influence combustion and heat transfer, as they're validated on conventional engine testbeds. This creates a gap in accurately simulating heat transfer for marine SI engines, underscoring the need for targeted model assessment. Here, these heat-transfer models are applied, compared, and evaluated under full-scale, multi-cylinder, lean-burn conditions to assess modeling accuracy and sensitivity to key parameters. By identifying which correlation best predicts in-cylinder heat loss, this review lays the groundwork for more reliable thermal modeling and optimized natural-gas spark-ignition (NG-SI) retrofit strategies.

Acknowledgements

This work would not have been possible without the guidance and support of my supervisors, Professor Peter de Vos and Professor Thijs Vlugt. I am deeply grateful to Konstantinos Kiouranakis for his guidance and invaluable help throughout this work. I want to thank my family for their constant support, understanding, and love, without which this work would not have been possible. I would also like to thank my friends for their encouragement and motivation during the journey of this thesis. Special thanks to my friends from EFPT who were always there for me: Mo, Jack, Ezra, and Alessio. I am especially grateful to my girlfriend Elina for her support, patience and love, i could not have done this without her.

I dedicate this journey to my grandfather and to my friends who are no longer here with me.

Contents

Nomenclature

A_w	Surface area for heat transfer	[m^2]
a	Empirical exponent (dimensional analysis)	[-]
B	Cylinder bore diameter	[m]
C_1, C_2, C_3	Empirical constants in heat transfer correlations	[-]
$C_{\mathbf{ste}}$	Empirical constant (natural convection)	[-]
Gr	Grashof number (buoyancy-influenced convection)	[-]
h	Specific enthalpy of the gas	[$\mathrm{J/kg}$]
h, α_w	Convective heat transfer coefficient	[$\mathrm{W/(m^2\,K)}$]
k_g	Thermal conductivity of gas	[$\mathrm{W/(m\,K)}$]
m	Mass of gas inside the cylinder	[kg]
m	Empirical exponent (Reynolds number)	[-]
n	Engine speed	[rpm]
Nu	Nusselt number	[-]
P	Instantaneous in-cylinder pressure (with combustion)	[Pa]
P_1	Reference pressure	[Pa]
$P_{\mathbf{mot}}$	Motored in-cylinder pressure (without combustion)	[Pa]
Pr	Prandtl number (momentum/thermal diffusivity)	[-]
Q_w	Heat transferred to cylinder walls	[W]
R	Specific gas constant	[$\mathrm{J/(kg\,K)}$]
Re	Reynolds number	[-]
T	Gas temperature inside the cylinder	[K]
T_1	Reference gas temperature	[K]
T_g	Gas temperature for Bargende/Heywood correlations	[K]
T_w	Cylinder wall temperature	[K]
t	Time	[s]
v	Characteristic gas velocity	[$\mathrm{m/s}$]
v_p	Turbulence-enhanced gas velocity (gas motion + combustion effects)	[$\mathrm{m/s}$]
v_{mp}	Mean piston speed (mechanical piston motion)	[$\mathrm{m/s}$]
V_c	Clearance volume at TDC	[m^3]
V_d	Displacement volume	[m^3]
W	Work done by the system (gas on piston)	[J]
ΔU	Change in internal energy	[J]
φ	Crank angle	[°]

Acronyms

AFR Air–fuel ratio

ATDC After top dead center

BDC Bottom dead center

BTDC Before top dead center

CA Crank angle

CI Compression ignition

DI Direct injection

EGR Exhaust gas recirculation

EOC End of combustion

EVO Exhaust valve opening

HCCI Homogeneous charge compression ignition

ICE Internal combustion engine

IMEP Indicated mean effective pressure.

IVC Intake valve closing

LBSI Lean burn spark ignition

MAPE Mean absolute absolute percentage error

MFB Mass fraction burned

NG Natural gas

SI Spark ignition

SOC Start of combustion

TDC Top dead center

1

Introduction

Spark-ignition (SI) internal combustion engines (ICEs) are increasingly important for heavy-duty (HD) applications such as transportation and power generation, especially because of the growing demand of high-octane sustainable fuels. Natural gas (NG), in particular, has attracted attention thanks to its availability and potential to reduce the environmental footprint of ICEs. However, HD SI engines continue to face challenges with combustion abnormalities like misfires and knock, highlighting the need for further research to understand their behavior and improve performance. A distinct feature of ICE combustion is heat transfer, which accounts for a substantial portion of the fuel's chemical energy. These losses directly affect efficiency and combustion behavior. For example, excessive heat transfer can significantly deteriorate combustion performance, while lower heat loss levels raise knock risks which may damage engine components. To this end, accurate modeling of in-cylinder heat transfer is therefore critical for predicting performance reliably and promoting the development of strategies that can enhance efficiency and reduce emissions.

Advances in computational modeling have made engine simulations a mainstay of modern development, offering faster and more cost effective pathways than purely experimental campaigns. Yet simulation accuracy depends strongly on how heat transfer is modeled, because it shapes the predicted pressure, temperature, performance, and emissions. Experimental testing is expensive and time consuming, so simulations are indispensable for exploring designs and operating strategies. Despite decades of research, however, faithfully modeling in-cylinder heat transfer remains challenging due to its transient, turbulent nature. Numerous semi empirical correlations exist, each tailored to specific engines, datasets, or conditions but no universal model has emerged. The primary objective of this study is to assess and compare the predictive capabilities of established heat transfer correlations in the context of lean burn spark ignition (LBSI) natural gas engines, with a particular focus on heavy duty marine operation. A central challenge is that most correlations were derived from measurements on single-cylinder engines configured for conventional combustion strategies. By contrast, the LBSI concept combines diesel-like combustion chamber geometry (bowl-in piston) with SI flame propagation.

This converted engine raises important questions about the suitability of conventional heat transfer correlations for LBSI operation. Experimental data are used for validation, but all correlations are applied strictly in their published form without calibration to evaluate their accuracy in how close the predictions are to the measurements. Many single zone (0D) engine models rely on convective heat transfer correlations that were derived or tuned on single cylinder gasoline or diesel engines, rather than on HD, multi-cylinder, lean-burn marine NG–SI engines with bowl-in pistons and distinct in-cylinder flow regimes. As a result, the accuracy of these correlations for predicting marine LBSI heat loss remains uncertain and under-validated. This work addresses the gap via a controlled, head to head comparison under identical inputs. Accordingly, this study addresses two questions: which correlation best predicts in-cylinder heat loss under lean-burn marine NG–SI conditions, and how sensitive are those predictions to key parameters

With this scope and method, a fair assessment of correlation performance and parameter influ-

ence is enabled for lean-burn marine NG–SI operation. The report proceeds with a literature review, methodology, experimental setup, results, validation and sensitivity analyses, and ends with conclusions and recommendations.

2

Literature Review

2.1. Thermodynamic Cycles

Internal combustion engines (ICEs) dominate a significant portion of global industries and are utilized in various applications, including the automotive and maritime transportation sectors. Spark ignition engines and diesel engines have long been the primary types of ICE technologies. These heat engines generate power through cyclic operations , the analysis of which in real-world applications is inherently complex and challenging. To facilitate analytical study of these engine cycles, numerous assumptions and simplifications of complex physical phenomena are typically required. To simplify these complexities, first modeling efforts solely relied on simplified cycles with reversible processes, typically referred as the ideal cycle [1]. An idealized model enables the analysis of the effects of key parameters governing engine performance without involving complex details. Despite the simplifications, ideal cycles serve as a very useful reference for understanding and approximating actual engine cycles.

Notably, heat engines operating on fully reversible cycles, such as the Carnot cycle, achieve the highest theoretical efficiency. It is well-established fact that no thermodynamic cycle can surpass the efficiency of the Carnot cycle. Because most practical cycles deviate significantly from the Carnot cycle, it renders it unsuitable to be employed as a realistic model for actual engine operation. Each ideal cycle is associated with work production of the actual cycle with the aim to mimic it [1]. Ideal cycles exhibit internal reversibility, however, they are not necessarily externally reversible (Carnot cycle can be externally reversible). For this reason, the thermal efficiency of ideal cycles is lower than that of a completely reversible cycle running at the same temperatures. Nonetheless, the thermal efficiency of ideal cycles is viewed higher than that of actual cycles due to the ideal assumptions made in their analysis [1].

2.1.1. Overview of the reciprocating engines

The reciprocating internal combustion engine is one of the most enduring and versatile technological innovations, having played a critical role in development of modern transportation and power generation systems. Its robust design and adaptability have made it dominant choice across a wide range of applications, from automobiles and aviation to industrial machinery and, notably marine propulsion systems, where reliability and efficiency are essential. The engine power relies on the reciprocating motion of a piston within the cylinder from a bottom position, the bottom dead center (BDC) to the highest position, the top dead center (TDC) [1]. In the cylinder the piston moves back and forth between two specific points. The engine's stroke is the maximum distance the piston travels in one direction from TDC to BDC and bore is called the piston's diameter. Below the figure depicts the main parts of a reciprocating engine.

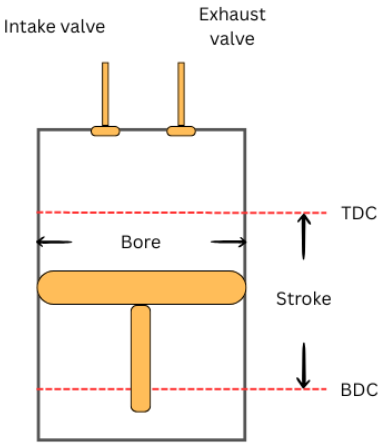

Figure 2.1: The basic components of a reciprocating engine [1]

ICEs can be categorized as spark-ignition (SI) engines or compression-ignition (CI) engines, based on how the combustion process takes place in the cylinder. The combustion of the SI engines relies on the flame creation from a spark plug, which subsequently propagates through an already mixture of fuel and air in the cylinder. On the other hand, in CI engines, fuel is typically injected separately from air in the cylinder at an environment of very high pressure and temperature close to TDC. Consequently, the fuel is evaporated, mixed with air, and spontaneously autoignite. The engines which are called four-stroke ICE, the pistons undergo four complete strokes (equivalent to tow mechanical cycles) in the cylinder, while the crankshaft rotating twice [1]. A picture below depicts the strokes and the p-v diagram of a four-stroke SI engine.

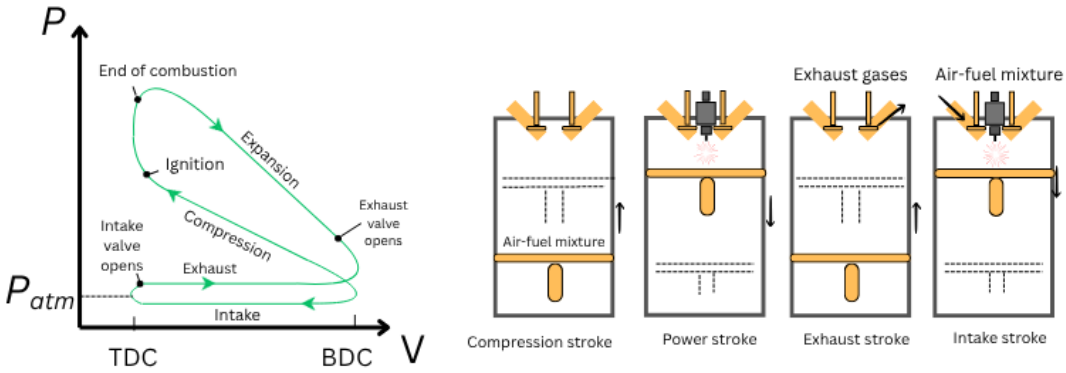

Figure 2.2: Actual cycle in spark ignition engines and the P-V diagram [1]

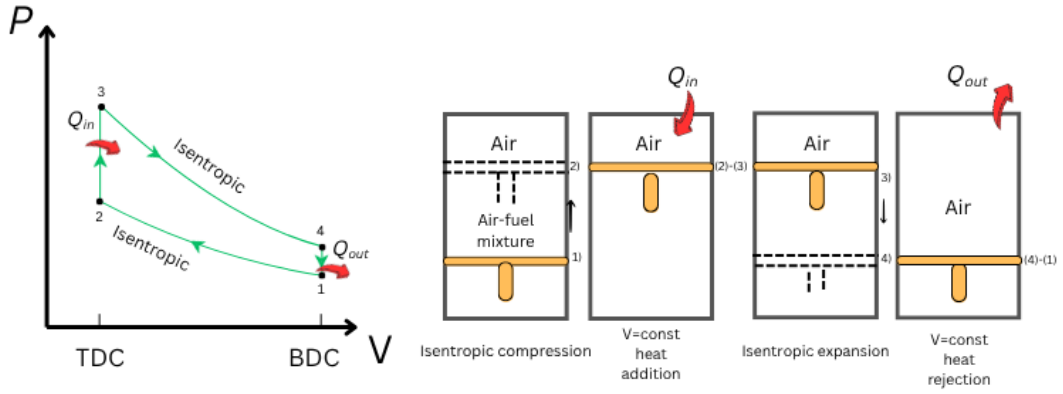

Figure 2.3: Ideal cycle in spark ignition engines and the P-V diagram [1]

In four-stroke engines, at first, the exhaust and the intake valves are sealed and the piston sits at the BDC, i.e., the lowest position of the piston. The piston rises when the compression stroke occurs and the mixture of air-fuel is compressed. Just before the piston gets to TDC (highest position of the piston), the mixture of air-fuel gets ignited by the spark plug [1]. The flame initiated from the ignition point propagates through the charge, leading to a rapid increase in pressure and temperature. The expanding high-pressure gases push the piston downward, rotating the crankshaft so as work is produced during the power stroke. At the close of the power or expansion stroke, the exhaust valve opens, enabling the pressurized combustion gases to escape the cylinder. This process, known as exhaust blow-down, allows the majority of combustion gases to exit the cylinder before the piston gets to BDC. However, since the cylinder still contains exhaust gases at BDC, the piston moves up to expel the remaining exhaust gases out of the cylinder. Following the exhaust stroke, the piston moves downward again to breathe and suck fresh air-fuel via the intake valve. During the exhaust stroke the pressure inside the cylinder is slightly higher than the atmospheric pressure, while in the time of intake stroke it is slightly lower [1].

On the other hand, two-stroke engines the four functions, described for four-stroke engines, are completed in two strokes. These two strokes are the compression and the power stroke. The crankcase is closed off, and the piston's outward movement helps pressurize the mixture of air-fuel inside the crankcase. Furthermore, the exhaust and the intake valves are substituted with openings positioned near the base of the cylinder wall. In the final phase of the power stroke, the piston reveals the exhaust port, enabling the partial expulsion of the exhaust gases [1]. Shortly after, the intake port is uncovered, letting the mixture of fresh air-fuel to flow in and push out the majority of the leftover exhaust gases in the cylinder. As the piston moves upward during the compression stroke, it compresses the mixture which is then ignited from the spark plug. The four-stroke engines are more efficient than the two-stoke engines. This is because the two-stroke engines have incomplete removal of exhaust gases and the loss of some mixture of fresh air-fuel along with the exhaust.

Although, the two-stroke engines are simple and affordable, they offer high power-to-weight and power-to-volume, making them perfect for applications where compactness and low weight are essential, e.g., in motorcycles. It is complicated for the actual four-stroke or two-stroke cycles to be analyzed thermodynamically. Although, by using the air-standard assumptions the analysis becomes easier. The cycle that emerges, which closely approximates the real conditions of operation, is the ideal Otto cycle. Although, at the evaluation of the power output in ideal Otto cycle, it is essential to recognize that, similar to the actual four-stroke SI engine, the ideal Otto cycle operates with four strokes [1].

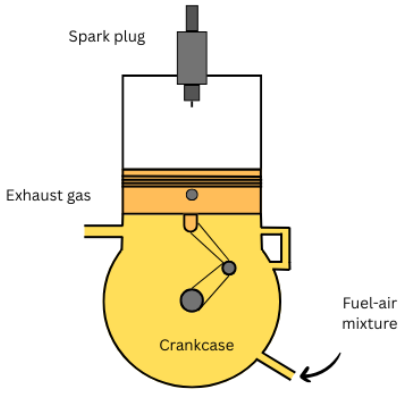

Figure 2.4: Schematic of a two-stroke engine [1]

The diesel cycle represents the ideal model for CI (compression-ignition) reciprocating engines. It differs in how the combustion is initiated. In SI engines, commonly referred to gasoline engine, the mixture of air-fuel is compressed to a point of temperature which is below the fuel's auto-ignition level, with combustion triggered by the firing of a spark plug. On the other hand, the CI engines, often referred as diesel engines function by compressing air to a temperature higher than the fuel's auto-ignition level. Combustion occurs immediately as the fuel is injected into the hot air, eliminating the need for the spark plug, which is replaced by a fuel injector. Gasoline engines typically compress a blend of fuel and air at the same time when compression stoke takes place. The compression ratio is constrained by the risk of auto-ignition, commonly referred as knocking [1]. This allows diesel engines to function at significantly greater compression ratios, usually ranging between 12 to 24. By eliminating the risk of knocking, diesel engines gain an edge over SI engines, as they can utilize less processed and consequently cheaper fuels[1].

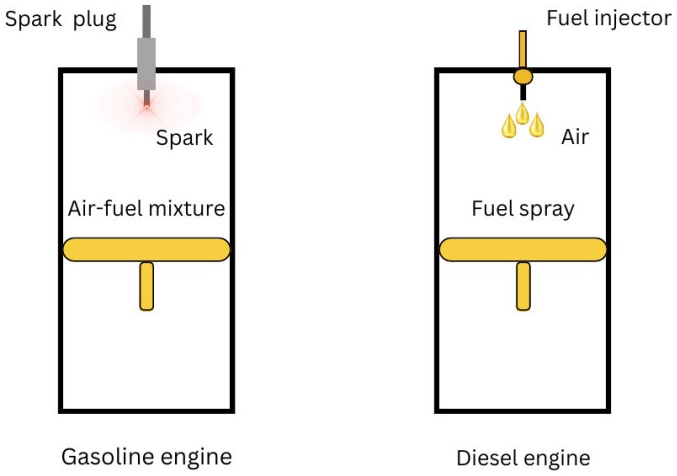

Figure 2.5: In diesel engine, is replaced by a fuel injector [1]

2.2. Cylinder Heat Transfer

Heat transfer is one of the most critical physical phenomena occurring during the in-cylinder processes of internal combustion engines (ICE). There are three heat transfer mechanisms: conduction, convection and radiation. Conduction occurs within the solid engine components, such as the cylinder walls and piston, with heat moving from regions of higher to lower temperatures. The convective mechanism involves heat transfer between the engine's solid surfaces and the adja-

cent fluids such as the air-fluid and coolant. Heat transfer by radiation is typically of smaller scale than conduction and convection, and it typically occurs at very high temperatures. The main factors that influence heat transfer are the geometry of the engine, including shape and size of the combustion chamber, surface to volume ratios, operating conditions, such as engine speed and air-fuel ratio, and material properties [2]. Figure 5.8 illustrates the use of the three heat transfer models (coupled) in order to obtain the heat transfer and temperature calculations.

- Gas to wall
- Wall to wall
- Wall to liquid

The gas to wall heat transfer model represents the fundamental methodology for simulating the thermal exchange between the high temperature gases inside the combustion chamber and the surrounding boundaries, such as the piston crown, cylinder head, and cylinder liner. This type of heat transfer also extends to the intake and exhaust sections of the engine where the temperature remains significant. The gas to wall modeling plays a critical role in determining the instantaneous heat flux from gas to walls, which directly affects the temperatures in the cylinder, the efficiency of the engine and the thermal load of components. In contrast, wall to wall heat transfer models are used to calculate the conduction of heat within the solid engine components themselves. These include piston, cylinder head, valves and cylinder walls where thermal energy absorbed at the surface is distributed internally. This conduction modeling is essential for capturing temperature gradient within materials, which influence mechanical stress and the long term durability of the engine parts. The third modeling approach, known as the wall to wall liquid heat transfer model, focuses on the dissipation of heat from the engine structure to the surrounding cooling fluids (coolant) in the water jackets and the lubricating oil in the crankcase [3]. At the figure below is illustrated the use of the three heat transfer models (coupled) in order to obtain the heat transfer and temperature calculations.

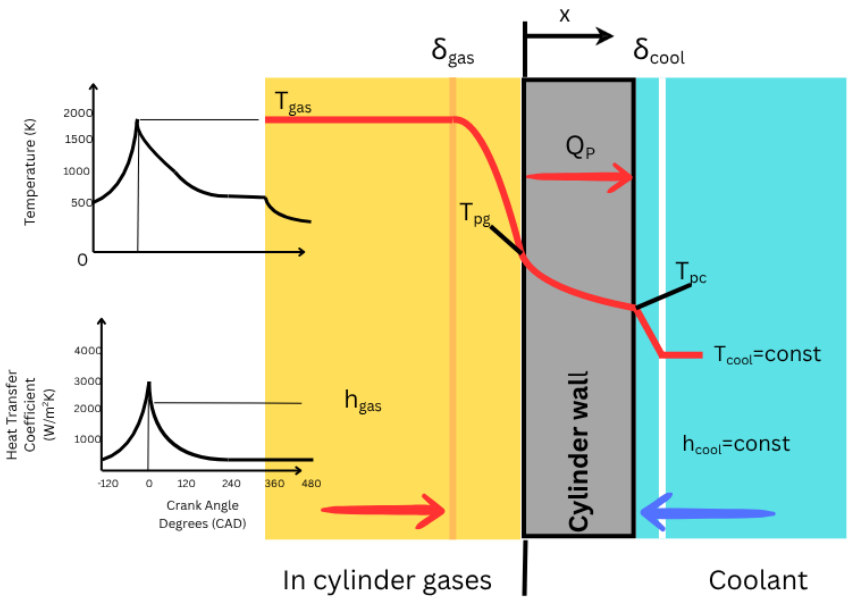

Figure 2.6: Illustration of combination for different heat transfer approaches [3]

However, complete and catholic convective heat transfer correlations have not been developed. The available correlations derive from experimental energy analyses of engines under limited operating conditions. Heat transfer in the engine cylinder occurs because the parts within the cylinder need to be kept at temperatures much lower than the cylinder gases, particularly during the phases

of the cycle with high temperatures. To achieve this, it is necessary to cool the components of the engine. Generally, heat flows from hot gases to the cylinder walls which are colder. At certain moments, however, the gases within the cylinder might be cooler than cylinder's components resulting in the heat flowing from the cylinder's walls to the gases [4]. The heat transfer within the cylinder is predominantly convective, although some thermal radiation may occur during soot formation, a phenomenon primarily concerning diesel engines.

In SI engines, the heat transfer by radiation is insignificant, hardly exceeding 4% of the total heat exchange [5]. On the other hand, this does not apply to diesel engines, where radiation can reach up to 10% of the total heat transfer, due to soot formation during combustion[5]. Therefore, because soot formation is typically negligible in premixed SI engines, the convective heat transfer is typically considered as the main mode of cylinder heat transfer. At the cylinder walls, the heat is transmitted via the metal (of the walls) and dispersed into a cooler medium, such as liquid coolant and air. The heat moves from the metal to the cooling medium mainly by means of convection. The heat transfer in the cylinder is highly complex due to the non-homogeneous thermodynamic, chemical and physical properties in the combustion chamber, especially during combustion [4]. The general expression for cylinder heat transfer is:

$$\dot{Q} = h_{\text{tm}} h_c A \left(T - T_{\text{wall}}\right) \tag{2.1}$$

The $\dot{Q}$ symbolizes the total heat transfer rate, h_c denotes for the coefficient of the convective heat transfer, *A* represents the area of the surface of the heat transfer, (T - T_{wall}) is the difference of the temperature between the wall temperature and the gas temperature, and the term h_{tm} is the "heat transfer multiplier." The parameter of h_{tm} will set as 1.0 unless situations arise where the effect of the heat transfer rate on engine efficiency is examined.

The Nusselt number Nu is a function of the Reynolds number Re, where a and b are empirical constants. The equation captures the dependency of the heat transfer coefficient on the fluid motion and thermal properties.

$$Nu = \frac{h_c L}{k_{gas}} = aRe^b = a\left(\frac{VL}{\nu}\right)^b \tag{2.2}$$

The thermal conductivity for gases is depicted by k_{gas}, the coefficient of convective heat transfer is h_c, Re is the Reynolds number, the variables "α" and "b" represent experimental estimations. The parameters "V" and "L" are the characteristic velocity and length and ν represents the kinematic viscosity. The engine bore is most of the times the characteristic length, the piston speed is represented most of the times from the characteristic gas velocity in the cylinder. However, the speed of the piston is not the most reliable indicator of gas velocity, particularly during events like combustion where it fails to capture the complex dynamics of the gas movement. This selection of piston speed is often used because of practical approximation, largely due to the fact that precise data on the gas velocities is unavailable.

2.3. ICE Simulation Methods

Growing global concern over greenhouse gas emissions has led to the adoption of increasingly stringent regulations governing ICE emissions. This regulatory pressure is driving researchers to accelerate the development of more sustainable propulsion systems [6]. Traditionally, the experimental studies have been the primary method for engine development. However, cost and complexity of experiments, combined with the ever-increasing computation power, engine simulations have become an integral part of research and development of ICEs. The precision of these simulations is largely determined by the precision of the fundamental models [7] [8]. The research in cylinder heat transfer of ICEs started some decades ago, driven by the need to optimize engine design parameters. This focus derives from heat transfer's critical influence on thermodynamic

efficiency, thermal loading, and emission characteristics in ICEs. The prediction of heat transfer remains an essential part in simulating engine behavior.

Through a more accurate modeling of heat transfer, alternations in design can be assessed, reducing the need for testing and construction, thereby accelerating the development phase. This process can further allow for faster and more cost-efficient engine designs with improved thermal characteristics. There are numerous approaches to modeling and measuring heat transfer in ICEs. Thermodynamic models are essential tools for engineers and researchers. They help design engines that meet emissions regulations while delivering strong performance [9] [10] [11]. Noways, with the rise of alternative fuels and technologies like exhaust gas recirculation (EGR), it's becoming harder to predict how these factors affect the engine behavior. That is the reason why the models must accurately simulate how different fuels influence combustion. Thermodynamic models are often used to simulate the closed cycle of spark ignition (SI) and compression-ignition (CI) engines, and they can be classified into three types [12]: zero-dimensional, quasi-dimensional, and multi-dimensional models.

Zero-dimensional models are trustworthy at accurately estimating the in-cylinder pressure; however, they fail at giving details over the temperature variation in the cylinder. This limitation comes from the assumption of a single uniform bulk-gas temperature throughout the cylinder, which simplifies the complex gradient present during combustion. In contrast, the multi zone model can provides with a more accurate prediction about the local temperature in the cylinder. The zero- and quasi-dimensional model are typically referred as phenomenological models, where the equations forming the core framework of these model are grounded in mass and energy conservation principles, depending on exclusively on the time variation leading to ordinary differential equations [12]. Multidimensional models, often categorized as computational fluid dynamic (CFD) models, constitute a higher-fidelity modeling framework for ICE analysis. The models rely on the solution of the Navier-Strokes equations [12].

2.3.1. Multi-dimensional Modeling

Simulation combustion with multi-dimensional computationally fluid dynamics(CFD) models has been a critical domain of research, with continuous progress in developing advanced physical and chemical modeling methodologies [13]. An accurate analysis of the temperature field is essential to avoid thermal failures. Measuring instantaneous heat fluxes (gas-to-wall) experimentally is highly complex , 3D-CFD simulations of the cylinder procedures are crucial for analyzing the total heat which is transferred to the cylinder walls.

An accurate estimation of thermal loads is essential and it can be obtained through 3D CFD simulations. Moreover, experiments and simulations can be combined so as the optimum estimation of thermal loads can be achieved. Evaluating the thermal energy acting on the components exposed to the combustion chamber is a demanding task and very hard to measure experimentally. Measuring instantaneous heat flux generally necessitates advanced and very expensive sensors (which are impractical for moving elements such as pistons). Alternatively, with recent technological progress, specialized thermocouples are able to measure the temperature of surfaces on the engine parts, including those in motion. These fast-response devices are called ”Thin Film Gauges” (TFG), can be positioned on the valve face or piston to capture localized temperatures, which after processing, can deliver precise heat flux data [14]. It has to be noted that, a close match between the simulated thermal field and the experimental measurements (taken with thermocouples) is used to verify the effectiveness of the simulation.

Furthermore, Nijeweme at [15] examined thoroughly the heat transfer in the cylinder, using both numerical simulations and an experimental methodologies. Nuutinen at [16] mentioned that in commercial CFD provides two primary methods for modeling the convective heat transfer in SI engine within the framework of RANS. The first method utilizes a wall function paired with a high Raynolds number turbulence model, which minimizes the need for a dense near wall mesh, thereby reducing computational expenses while approximating the flow and heat transfer near the walls. The second method involves employing a finer computational grid combined with either a low-Raynolds number or a turbulence model which is two layer, allowing for detailed spatial resolution of temperatures and velocities profiles in the near-wall region. While this method achieves high resolution and accuracy, its computational cost is impractical. As a result, analytical wall function remains the predominant choice in CFD methodologies. Research by authors [17] [18] [19] [20] indicates that the fusion of 3D-CFD in cylinder modeling with CHT (conjugate heat transfer) models delivers an accurate representation of the engine’s thermal profile.

CHT modeling concurrently solves the equations of energy for the solid phase and the governing equations for the fluid phase in the cylinder. This approach provides time-accurate predictions of heat flux and a dynamic temperature profile on the wall, resulting in more accurate evaluations of heat loss and it’s impact on in-cylinder combustion. Lei Zhang at [21] embedded a solid domain heat transfer into KIVA-4V code, enabling concurrent evaluations of the thermal fluid behavior and wall heat transfer in the cylinder. The author introduced a vertical segmentation strategy for the mesh sector to decrease the computation time. The thermal fluid dynamics equations (momentum, mass, and energy conservation , combined with several sub-models) are adjusted to compute heat transfer in the solid phase at the cylinder (head, liner, piston).

2.3.2. Numerical model description

Thermodynamic Cycle Models

The thermodynamic cycle model (TCM) can depict the internal combustion engines (ICE) as an open thermodynamic system, which can be represented using a single zone model or a complex of multiple thermodynamic systems, such as a two-zone or multi-zone model.

Because the pressure equalizes rapidly within the small volume of cylinder's engine, it is assumed that the pressure varies only with time τ and the crankshaft angle ϕ. It is also considered that the pressure is independent of the spacial coordinates (x, y, z). The TCM is employed to analyze the energy dynamics of the combustion within the ICE. It is used in cases where the gas parameters are considered to be uniform across the spatial coordinates (x, y, z) and depends solely on time and on crankshaft angle [22]. TCM is also used for the examination of the toxic emissions that are generated during combustion of the ICE [22].

The thermodynamic models are applied to address two key problems, the first one is related to predicting the variation of the pressure within the cylinder depending on time or crankshaft angle, built on a predetermined amount of energy released during the combustion $Q_x(\phi)$ and the heat which is transferred through the walls $Q_w(\phi)$. The second one is related to calculating the heat energy $Q_x(\phi)$ which is released during the combustion, using the predetermined pressure p(ϕ) which has been calculated either from computational data or experiments. Moreover, it is necessary to determine the heat transfer through the walls $Q_w(\phi)$. If these parameters have been obtained, then the total heat transfer dQ can be determined accordingly.

$$dQ = dQ_x - dQ_w \tag{2.3}$$

There are three equations that are used on the TCM type.

1. The first equation is the the first law of thermodynamics, as applied to the combustion chamber, states that the variation in the internal energy within the cylinder corresponds to the total of the work which is performed by the piston, the heat exchange, and the enthalpy carried by the gases entering or leaving the system.

$$\Delta U = Q + W + H_{\text{in}} - H_{\text{out}} \tag{2.4}$$

2. the ideal gas law

$$p = \frac{mRT}{V} \tag{2.5}$$

3. Mass conservation law

$$dm = \sum_i dm \tag{2.6}$$

Zero-Dimensional Models

The zero-dimensional models, also known as single-zone models, belong to thermodynamic cycle models (TCM). They are derived from the principles of mass and energy conservation within the engine's combustion chamber. These models typically employ a predefined mass burning rate, with the Wiebe function being the most commonly used example. However, the burning rate must be determined empirically for each specific engine operating condition, relying on prior experimental data or practical experience. Since it is not explicitly formulated in terms of physical attributes such as fuel characteristics or engine configuration, adapting these models to varying operational scenarios becomes more complex and less accurate [12]. Rashedul et al. [23] implemented a single zone framework to examine convective heat exchange within an SI engine running on bio ethanol. This thermodynamic modeling framework applies a single-zone methodology and is grounded in fundamental principles of the first law of thermodynamics.

Amel Djouadi at [24] used simulations to make an analysis for methane-hydrogen combustion, incorporating the specific heat ratio and heat transfer coefficient models. It was examined on a four-stroke SI engine using single zone models based on cylinder pressure data. Junseok Chang at [25] developed a convective heat transfer correlation for a gasoline-fueled HCCI engine using single-zone thermodynamic model. In their approach, the entire combustion chamber is treated as one lumped control volume with spatially averaged pressure and temperature, and heat release is calculated via a 0D first-law analysis coupled to fast-response wall heat-flux measurements. Sary Awad at [26] developed a single-zone thermodynamic model to analyze combustion in a single-cylinder diesel engine and create general equation for predicting the performance of the engine using various fuels. This model included submodels for gas and air flow, air/fuel mixture ignition, fuel burning rate and heat losses. Anand M Shivapuji and S Dasappa [27] examined experiments and modeling of producer gas, a bio-derived low energy fuel, in an SI engine. The study estimates producer gas-specific Wiebe coefficients from experimental heat release data, finding an efficiency factor of 2.4 and a shape factor of 0.7 for 2% to 90% burn duration. The standard Wiebe coefficient were used in 0D model and led to large deviations in simulation results, but producer gas specific coefficients yielded accurate predictions for both 6-cylinder and 3-cylinder engine configurations.

Galindo at [28] developed Wiebe parameters for a two-stroke engine, establishing a correlation between combustion duration and shape factor based on experimental studies conducted across various engine operating conditions. Melih Yildiz and Bilge Albayrak Ceper at [29] examined the comparison between single and double Wiebe function in a 0D model for methane methane-hydrogen fuels, analyzing the in-cylinder pressure and gross indicated mean effective pressure. Parameters were estimated using the least squared method, fitting mass fraction burned curves via the Rassweiller-Withrow method.

Two-Zone Models

The two-zone combustion model builds upon the foundation of the single-zone model by introducing additional thermodynamic premises that enhance its predictive accuracy, particularly in relation to in-cylinder processes, engine performance, and exhaust emissions. While it remains a TCM like its single-zone counterpart, the two zone offers a more detailed representation of the combustion chamber. To support this level of detail, several assumptions are introduced and are outlined below.

- The separation the cylinder volume (V) and the working fluid mass (m) into two distinct regions: the unburned section (m_u, V_u) and the combustion section (m_b,V_b), separated by a narrow reaction interface (flame boundary). This segmentation enables a more detailed depiction of combustion phenomena. The combustion chamber's division is shown below:

$$V = V_u + V_b \tag{2.7}$$

$$m = m_{\text{fuel}} + m_b = m_{\text{air}} = m_u + m_b \tag{2.8}$$

- The cylinder's internal pressure remains consistent at all time.
- Each zone has a consistent temperature throughout and no thermal exchange takes place between the zones.
- Inside the cylinder the working fluid is uniform in composition and consists of air, fuel vapor, and leftover combustion gases.
- There is a different heat transfer coefficient for every zone. Also, there is a unique contact area for each zone.

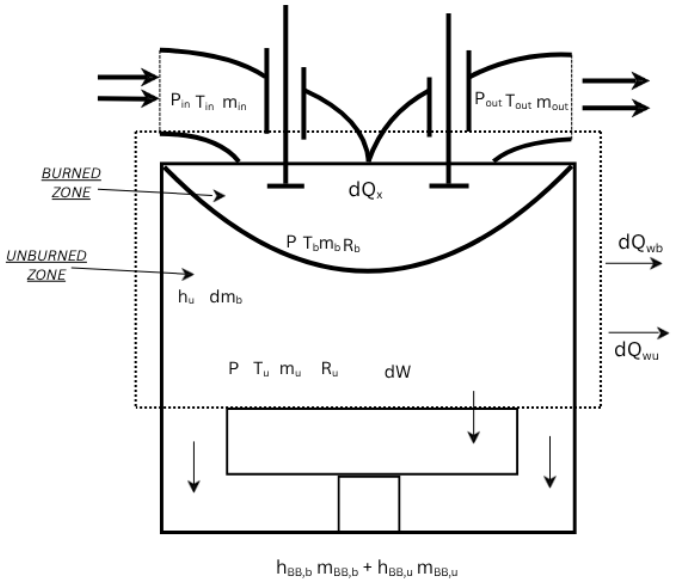

Figure 2.7: Two-Zone Combustion Model Representation [22]

The division of the combustion chamber into two zones allows for a more precise prediction of the temperature in the cylinder. As a result many research studies focus on two-zone modeling while also tackling challenges that are similarly addressed by single-zone approaches. Morteza Fathi at [30] developed a single and a two-zone model including a hybrid approach. Experimental data validate the assumption of the charge homogeneity, confirming that neglecting injection-induced stratification is reasonable. Both models accurate predict DI-HCCI performance, though the single-zone approach overestimates maximum pressure and power. Mohand Said Lounici at [31] examined the evaluation of different correlations and heat transfer area calculation methods using computer simulations and experimental validation. The results of this study also highlighted that the method of calculating the burned zone heat transfer area has minimal impact and the optimization heat transfer modeling enhanced the efficiency of two-zone simulations for natural gas SI engine. Yann G. Guezennec and Wajdi Hamama at [32] conducted a two-zone crank-angle resolved pressure analysis using variable composition and properties. The heat transfer correlation is iteratively adjusted until the burn mass fraction aligns with combustion efficiency from exhaust data. This reverse modeling ensures agreement with measured data and self-calibrates the heat transfer correlation for the tested engine and conditions. This test was operated on SI engine, providing an efficient an evaluation of the combustion characteristics

Heat transfer sub-models

The heat transfer sub-model is one of the most crucial components of the thermodynamic models, as it estimates the heat transferred from the cylinder charge to the walls. To this end, this study shifts its focus on the convective gas-to-wall heat transfer model incorporated in TCMs. This heat transfer process in the combustion chamber derives from the Newton's cooling law, expressed as:

$$dQ_w = \alpha_w A_w (T - T_w) dt \tag{2.9}$$

While Equation (2.9) describes heat transfer rates in the time domain. As crank angle domain is typically used in ICEs and TCMs, Equation (2.10) converts the time to the crank angle domain.

$$dt = \frac{d\phi}{6n} \tag{2.10}$$

where time (t) is measured in seconds, (n) is specified in revolutions per minute (rpm), and (ϕ) is in degrees.

To evaluate the heat losses in the cylinder during an engine cycle, the heat transfer coefficient is the primary value to be determined. The most significant factor of the heat transfer sub-model is the coefficient of heat transfer α_w. Over time, extensive research has explored gas-to-wall heat transfer in spark-ignition (SI) engines and compression-ignition (CI) engines, leading to the formulation of numerous correlations that estimate the instantaneous heat transfer coefficient. These correlations aim to model the spatially averaged heat transfer in the cylinder. There has been a variety of semi-empirical formulas applied to estimate this heat transfer coefficient.

Heat transfer correlations

During combustion, in-cylinder charge experiences a sharp temperature rise, which can reach up to 2800K [33]. This extreme heating causes the gases to expand, and rapidly increase their velocity. This is the stage that most heat exchange takes place [33]. Between the gases and the chamber walls the heat transfer is inconsistent and fluctuates over time, making it hard to establish a precise estimation. However, there have been several applied techniques that aim to determine this heat transfer process. An evaluation of the heat transfer coefficient can be done by implementing some of the heat transfer correlations. These correlations can be divided into two categories, based on the assumption about the source of the heat transfer.

Natural convection assumption

Initial heat transfer models for engines were based on the assumptions of natural convection, where fluid motion is driven by temperature differences. Under this approach, the heat transfer coefficient is expressed in a dimensionless format as follows:

$$Nu = \mathrm{Cst}\,(Gr \times Pr)^n \tag{2.11}$$

The first model, proposed by Nussenlt in 1923, originated from an empirical correlation based on spherical bomb experiments [34]. Brilling and Eichelberg later modified and adapted this model using experimental data from ICE's [35] [3]. These early models were significant in initially capturing the influence of key engine variables such as gas temperature, rotational speed and pressure. However, their applicability proved limited. Woschni later pointed out, the accuracy of these correlations inherently low, noting that they provide only rough approximations. Consequently, this method was eventually replaced by dimensional analysis approaches that incorporate forced convection effects. Forced convection results from external motion like piston movement [31, 36].

- Eichelberg heat transfer coefficient [36]

$$h = 7.67 \times 10^{-3}\,(V_{mp})^{1/3}\,(P \times T_g)^{1/2} \tag{2.12}$$

Forced convection assumption

Since the assumption of natural convection is inadequate, the correlations based on it are difficult to apply across different engine types. Therefore, various researchers pursued experimental investigations based on the forced convection, recognizing its superiority accuracy duo to the role of external mechanical forces in driving fluid motion within the chamber. Dimensional analysis of turbulent flow, linking the Nusselt, Reynolds, and Prandtl numbers, formed the basis of these investigations. Through quasi-steady engine experiments, researchers derived empirical correlations for heat transfer across different types of ICEs, including SI and CI engines. The Nusselt number is typically formulated in a standardized manner, incorporating specific assumptions.

$$Nu = a \times Re^m \times Pr^n \tag{2.13}$$

By replacing the Nusselt and Reynolds numbers in terms of physical properties, the overall heat transfer coefficient is affected by factors such as characteristic length, pressure, temperature, and characteristic velocity. A scaling parameter is typically employed to adjust the coefficient, ensuring the compatibility with specific engine configuration. Several researchers have proposed

different values for the exponent m. Apart from Woschni correlation, most of these models use time-averaged velocity that is directly proportional to the mean piston speed. The forced convection assumption is a more realistic approach because the motion of the fluid in the chamber is driven by external mechanical movements [37].

- Woschni heat transfer coefficient

  Woschni is the first heat correlation discussed in this study [38]. The correlation of Woschni is well established and extensively used for SI and CI engines. Moreover, this correlation offers the most comprehensive method for estimating the convective heat transfer. Unlike other correlations that assume a steady velocity of gas throughout the engine cycle, the approach of Woschni incorporates the acceleration of gas flow inside the cylinder, particularly during the combustion process.

$$h = C_1 \cdot \left[B^{-0.2} \cdot p^{0.8} \cdot \left((C_2 \cdot v_{mp}) + C_3 \cdot \frac{V_d \cdot T_1}{P_1 \cdot T_1} \cdot (P - P_{mot}) \right)^{0.8} \cdot T^{-0.53} \right] \tag{2.14}$$

- Hohenberg heat transfer coefficient

  Hohenberg asserted that the correlation of Woschni undervalues the heat transfer coefficient and overstates it during combustion. Additionally, he emphasized the challenges associated with its implementation [35]. Building upon the findings of Woschni, Hohenberg developed the following correlation.

$$h = C_1 \cdot V_c^{-0.06} \cdot p^{0.8} \cdot T^{-0.4} \cdot (C_2 - v_{mp})^{0.8} \tag{2.15}$$

- Annand heat transfer coefficient

  In contrast to the previous two correlations, firstly developed for Diesel engines and later adapted for SI engines, the correlation of Annand was directly developed from experiments on SI engines. The Annand methodology presumes that the gas velocity remains unchanged and uniform throughout the engine cycle and equal to the mean piston speed [39]. The heat transfer coefficient is computed as indicated below.

$$h = C_1 \cdot \frac{k_g}{B} \cdot \mathrm{Re}^{0.7} + 4.3 \times 10^{-9} \cdot \left(\frac{T_g^4 - T_w^4}{T_g - T_w} \right) \tag{2.16}$$

  The second term of the equation considers the impact of radiation which is neglected in SI engine studies.

- Sitkei heat transfer coefficient

  The heat transfer correlation of Sitkei is an empirical model to calculate the heat transfer coefficient in SI engines. It enhances previous models by incorporating factors such as pressure of cylinder, gas temperature and volume making it versatile across different engine conditions [40]. The Sitkei heat transfer correlation is shown below.

$$h = 2.36 \times 10^{-4} \cdot (1 + C_1) \cdot \frac{(P \cdot v_{mp})^{0.7} \cdot A^{0.3}}{T^{0.2} \cdot (4V_c)^{0.3}} \tag{2.17}$$

- Han heat transfer coefficient

  Han introduced an empirically derived expression for the instantaneous heat transfer coefficient specifically targeting SI engines and relying on robust dataset obtained through both physical experimentation and CFD modeling. He presented an empirical relationship for h that changes with engine's crank angle offering improved accuracy in tracking real-time variations compared to conventional models [41]. The heat transfer correlation of Han is illustrated below:

$$h = 687\, P^{0.75} U(\theta)^{0.75} D^{-0.25} T^{-0.465} \tag{2.18}$$

$$U(\theta) = 0.494\, V_p + 0.73 \times 10^{-6} \left(1.35 P \frac{dV}{d\theta} + V \frac{dP}{d\theta} \right) \tag{2.19}$$

- Bargende heat transfer coefficient

  The heat transfer model of Bargende is an improved empirical correlation developed for SI engines. It builds upon Woschni's heat trasnfer model by incorporating a turbulence offset and modifying the gas velocity term to better capture transient effects and high speed operation [42]. The heat transfer coefficient is depicted below:

$$h = 253.5 \cdot V^{-0.073} \cdot p^{0.78} \cdot \bar{T}^{-0.477} \cdot w^{0.78} \cdot \Delta \tag{2.20}$$

- Heywood heat transfer coefficient

  The Heywood heat transfer model is another versatile empirical correlation, which expresses the heat transfer coefficient as a power-law function of in cylinder pressure, temperature and gas velocity [43]. The heat transfer correlation is shown below:

$$h = 3.26 \cdot B^{-0.2} \cdot P^{0.8} \cdot T^{-0.53} \cdot v^{0.8} \tag{2.21}$$

  A variety of empirical models exist to estimate the heat transfer coefficient in SI engine simulations. The table below summarizes the most relevant models considered in this study, along with their recommended use cases, applicable speed ranges, and modeling characteristics.

Model (Author)	Best Suited For	Engine Speed Suitability	Engine Configuration
Woschni (1967) [38]	SI and CI engines under general conditions	All speeds	Single-cylinder research diesel engine
Hohenberg (1979) [35]	SI engines during combustion	Medium to high RPM	Multi-cylinder automotive diesel engine
Annand (1963) [39]	High-load SI engines	All speeds (better at high load)	Single-cylinder gasoline & diesel engines
Eichelberg (1939) [36]	Simplified or early SI models	Low RPM	Single-cylinder motored gasoline engine
Sitkei–Ramanaiah (1975) [40]	Motored cycles or academic use	Low to medium RPM	Single-cylinder DI diesel engine
Han (2019) [41]	Modern SI engines; crank-angle resolved analysis	All speeds	Single-cylinder SI engine (methane/H_2 blend)
Bargende (1991) [42]	High-speed or turbocharged SI engines	High RPM	Multi-cylinder SI engine
Heywood (1988) [43]	Calibration, reference, or flexible modeling frameworks	All speeds	Generalized automotive SI engine

Table 2.1: Comparison of Heat Transfer Models for SI Engines

The heat correlations shown in the table are widely used and validated in single-cylinder engine studies and have been applied across various engine types for heat transfer predictions. Their implementation in a multi-cylinder marine SI engines allows direct assessment of each model's

performance when scaled to a heavy-duty, multi-cylinder marine engine, highlighting relative accuracy, computational cost, and sensitivity to lean-burn operating conditions. The model of Woschni was chosen as a benchmark due to its widespread adoption and compatibility with commercial engine tools. To enhance accuracy during the combustion phase, the Hohenberg model was included, particularly for its improved handling of pressure and piston-speed effects. For more modern data-driven insight, the Han model incorporates crank-angle-resolved behavior validated by CFD and experimental data. Moreover, the Annand model was incorporated to capture the convective heat transfer effects (there is also the ability to capture the radiative heat transfer if it is not negligible). The Bargende model, designed for high-speed SI engines, Bargende's model captures elevated turbulence and swirl effects common in heavy duty applications. Its application is suited to environments with access to high resolution flow data. Heywood's model uses a generic power law based on Reynolds and Prandtl numbers, offering broad applicability. However, its reliance on tuned coefficients without explicit geometry or piston speed terms limits its accuracy in uncalibrated, lean burn marine SI engines. Sitkei Ramanaiah's model is unique in explicitly incorporating combustion chamber volume, hence piston bowl geometry into its heat transfer correlation, making it particularly sensitive to variations in chamber shape. Eichelberg's model is one of the earliest empirical correlations, characterized by its simplicity and lack of combustion phase or piston motion considerations. Eichelberg's model is computationally trivial and represents a "lower bound" estimator. By comparing advanced correlations against this minimal approach, we can clearly gauge the performance gains afforded by modern, physics based models.

2.4. Conclusion

This literature study aimed to explore various types of heat transfer models developed for thermodynamic simulation in internal combustion engines (ICEs). In particular the study investigated the heat transfer models and their application in different engines. Given that a significant portion of the energy released during combustion is lost to the engine walls, understanding and accurately modeling the heat transfer is essential for for research and development efforts to improve the performance of these engines.

Although thermodynamic models (single-zone, multi-zone) are widely employed in spark ignition (SI) and compression ignition (CI) engine simulations, there remains a notable gap in the literature concerning systematic studies explicitly quantifying the accuracy, limitations and uncertainty associated with thermodynamic model simulations. Despite growing interest in natural gas-spark ignition (NG-SI) conversions to improve performance in marine applications, studies on heavy duty engines such as the lean burn spark ignition (SI) technology remain scarce. These engines display distinctive in-cylinder flow regimes that profoundly influence combustion and the heat transfer. Yet current heat transfer models are developed and validated on conventional engine testbeds. However, they cannot capture or assess these regime-specific effects on the combustion and the heat transfer, leaving a gap in accurately simulating the heat transfer for spark ignition engines applications and highlighting the necessity for dedicated model validation. Most of the studies are on single cylinder (smaller engines), which provide isolated diagnostic insights but they do not cover the full complexity of multi-cylinder operation. As a result, the thermodynamic models which are widely used in one cylinder SI engines, luck experimental validation under heavy duty multi-cylinder engines.

The research focuses on implementing and comparing heat transfer correlations within a thermodynamic modeling framework. These correlations were selected based on their relevance to convective gas to wall heat transfer. By simulating the engine behavior under consistent conditions and comparing against experimental data, the study will investigate the ability of different models to predict heat loss accurately. This thesis will address the following questions: Which heat transfer correlation delivers the most reliable in-cylinder heat loss predictions under lean, heavy duty conditions. How sensitive are those heat-loss predictions to variations in the key parameters of each correlation, and which parameter exert the greatest influence.

Ultimately, this work contributes to narrowing the literature gap related to heat transfer modeling in real multi-cylinder heavy duty NG SI engine under lean conditions. It provides insights that can support the future development of more efficient and cleaner combustion systems through improved thermal modeling.

3

Methodology

3.1. Simulation Environment and Engine Model

In this study, the simulations were developed within the MATLAB and Simulink. A single-zone thermodynamic model is applied, which assumes spatially uniform pressure and temperature within the combustion chamber. This simplified modeling approach enables efficient and computationally fast simulations of the in-cylinder processes. It is well suited for evaluating the convective heat transfer coefficient, as it can approximate the overall thermal behavior without requiring complex spatial resolution.

The model simulates a four-stroke multi-cylinder lean-burn spark-ignition (LBSI) marine engine powered by natural gas. A closed in cylinder process is modeled, starting from intake-valve closing (IVC) to the point of exhaust-valve opening (EVO). The combustion process is modeled using the Wiebe function ans specifically a two stage Wiebe. The exact form and parameterization of this function is reported in section 3.2. The in-cylinder state is advanced at each crank angle by the closed-system first law

$$m\, c_v(T)\, \frac{dT}{d\theta} = \frac{\dot{Q}_{\mathrm{rel}}(\theta) - \dot{Q}_w(\theta)}{\omega} - p(\theta)\, \frac{dV}{d\theta}, \tag{3.1}$$

$$p(\theta) = \frac{m\, R\, T(\theta)}{V(\theta)}. \tag{3.2}$$

The parameter, $\dot{Q}_{\mathrm{rel}}$ is the heat release rate from the Wiebe model, and the convective wall loss is:

$$\dot{Q}_w(\theta) = h(\theta)\, A(\theta)\, [T_g(\theta) - T_w]. \tag{3.3}$$

The trapped mass m is considered constant between IVC and EVO, $V(\theta)$ and $A(\theta)$ follow the geometry of the engine. An ideal gas mixture with temperature dependent $c_v(T)$ (closed volume) is assumed. For consistent comparisons among different correlations, $A(\theta)$ and T_w are held common. The variations of pressure and temperature inside the cylinder is computed based on the first law of thermodynamics. Based on the first thermodynamics law, the governing equation was applied in the cylinder, which was considered as closed control volume. At each crank angle the model computed the change in internal energy, taken to account the heat release from combustion and heat transfer to the walls of the cylinder. The volume change was modeled as a function of the crank angle, and the working fluid was assumed to behave as an ideal gas. The main goal of the study was the evaluation of the convective heat transfer between the gas and the walls of the cylinder. Different correlations were used to approximate the heat transfer coefficient based on parameters such as pressure, temperature of the gas in the cylinder, volume of the cylinder and the velocity of the piston. The correlations which were used for the model are described in Section 3.2. All correlations are tested under the same conditions so as the models could be compared in terms of their performance.

Modeling assumptions

The single zone assumes spatially uniform gas temperature and composition, measured wall temperature, thermo-physical properties are temperature depended and no crevice heat transfer is assumed. Radiation is also neglected for the SI NG engine. The heat transfer analysis is studied for the combustion phase of the closed cycle. The computation window runs from the start of combustion (SOC) to the end of combustion (EOC). In this combustion analysis the gas-wall surface area is a crank angle depended. Head and crown areas are constant, while the liner area varies with the instantaneous clearance height. The valves-ports are ignored because they are closed during the (SOC)-(EOC).

3.2. Heat Transfer Correlations Implemented

Heat transfer is a major energy loss in internal combustion engines engines (ICE) and should be modeled accurately. A precise estimation of the heat transfer between the gas and the walls of the cylinder is necessary for predicting engine's behavior. In zero-dimensional thermodynamic models empirical formulas are used to compute the convective heat transfer. These correlations evaluate the instantaneous heat transfer coefficient as a function of pressure in the cylinder, temperature of the gas, piston speed and geometry of the combustion chamber.

As already highlighted, due to the fact that the single-zone thermodynamic models neglect the high resolution fluid dynamics, the heat transfer coefficient plays a substantial role for the prediction of the heat transfer between gas and walls of the cylinder. In this way, the choice of heat transfer correlation influences the predictions of pressures, temperatures and the overall heat transfer in the engine. To examine the effect of different heat transfer correlations, some of the most cited heat transfer models were applied in this simulation. The correlations differ in how complex they are, their assumptions and the treatment of gas motion and combustion. Each of the model which was examined, is presented in the following sections.

Woschni heat transfer coefficient

The correlation of Woschni is very popular and widely applied for calculations of the heat transfer coefficient in both SI and Diesel engines. This correlation is well known because of its simplicity and accuracy. Various correlations take for account that the gas velocity is constant during the combustion cycle, the correlation of Woschni presents a detailed method for estimating the convective heat transfer. In addition, it incorporates that the gas velocity rises within the cylinder during the combustion.

$$h = C_1 \cdot \left[B^{-0.2} \cdot P^{0.8} \cdot \left((C_2 \cdot V_{mp}) + C_3 \cdot \frac{V_d \cdot T_1}{P_1 \cdot T_1} \cdot (P - P_{\text{mot}}) \right)^{0.8} \cdot T^{-0.53} \right] \tag{3.4}$$

The modeling of gas velocity takes into account the movement of the gases during combustion and compression. However, it does not capture turbulence in high resolution.

Hohenberg heat transfer coefficient

According to Hohenberg the Woschni correlation underestimates the heat transfer coefficient during the compression phase and overestimates it during the combustion. Therefore, in many cases it often over predicts the average heat transfer during a cycle. In addition, Hohenberg pointed out some practical challenges which are related with the use of the correlation, these notices motivated him to come up with an alternative correlation.

$$h = C_1 \times V^{-0.06} \times p^{0.8} \times T^{-0.4} \left(C_2 + V_{mp}\right)^{0.8} \tag{3.5}$$

Annand heat transfer coefficient

Annand [39] proposed a compact, general heat-transfer model for reciprocating Diesel engines by analyzing published instantaneous wall flux data. He assumes a constant characteristic gas speed typically the mean piston speed (V_{mp}). Radiation is treated as a separate term and is negligible for the SI cases, so only the convective part is used.

$$\mathrm{Nu} = C\,\mathrm{Re}^{0.71} \quad \Rightarrow \quad h = \frac{k}{D_b}\,C\,\mathrm{Re}^{0.71} \tag{3.6}$$

$$h = \frac{k}{D_b}\,0.76\left(\frac{V_{mp}D_b}{\mu}\right)^{0.71}\left(\frac{p}{RT}\right)^{0.71} \tag{3.7}$$

with $C \approx 0.7 - 0.8$.

The equation 3.4 is taking to account only the convective part of the original correlation, the radiative part is neglected for SI engines.

Sitkei heat transfer coefficient

The heat transfer coefficient of Sitkei belongs to the same group as Woschni and Hohenberg equations. Initially it was developed on Diesel engine experiments. It provides an alternative equation for evaluating the convective heat transfer coefficient in internal combustion engines.

$$h = 2.36 \times 10^{-4}(1+b)\cdot\frac{(P \times V_{mp})^{0.7}\cdot A^{0.3}}{T^{0.2}\cdot(4V)^{0.3}} \tag{3.8}$$

The parameter b has different values depending on the type of combustion chamber.

- Direct combustion Chamber (0-0.03)
- Piston Chamber (0.05-0.1)
- Swirl Chamber (0.15-0.25)
- Pre-combustion chamber (0.25-0.35)

Bargende heat transfer coefficient

Bargende suggested an alternative version of Woschni's model by taking a different approach. The original Bargende heat transfer correlation presents the gas velocity term w, enhanced because of the the average kinetic energy$k$ is included. This approach is suitable for high-resolution simulations with spatial resolution or multi-zone models. Due to the fact that this thermodynamic model is single zone, a detailed turbulence modeling is not feasible. In single-zone thermodynamic modeling, spatial gradients and local velocities variations cannot be evaluated. In this way, turbulent effects are neglected or simplified. In this study the turbulent kinetic energy k was set constant so as to achieve computational efficiency and consistency with the single zone assumption. This assumption is based on the fact that k varies during the combustion. By setting k constant the model preserves the effect of turbulence on heat transfer through a simplified velocity term, avoiding to include the complex turbulent transport modeling. In addition, Bargende included a combustion factor Δ, to account for combustion effects. This term includes the effect of temperature differences between the wall of the cylinder and both the burned and unburned gases. As a result Bargende's correlation requires multi-zone model to distinguish between the burned and the unburned regions. However, since the study is developed on a single-zone thermodynamic model, there is no distinction burned and unburned zones, so the Δ combustion term is not included. Below is the original correlation of Bargende.

$$h = 253.5\cdot V^{-0.073}\cdot p^{0.78}\cdot \bar{T}^{-0.477}\cdot w^{0.78}\cdot\Delta \tag{3.9}$$

Below as $\bar{T}$ is mentioned the relevant gas temperature at which gas properties are computed, the estimated average temperature within the boundary layer is:

$$\bar{T} = \frac{T_G + T_w}{2} \tag{3.10}$$

The effect of turbulence on heat transfer is represented in the velocity term w, which is also including the kinetic turbulent energy. The parameter S_p is the instantaneous piston velocity and it is considered to be proportional with the cylinder's average gas velocity:

$$w = \frac{1}{2} \cdot \sqrt{\frac{8}{3} \cdot \bar{k} + \bar{S}_p^2} \tag{3.11}$$

As it is highlighted already, the combustion term Δ is taking into account the flame propagation, dividing the combustion chamber into burned zone V_b and unburned. zone V_u. Two sub-terms $[\mathbb{A}] \propto V_B/V$ and $[\mathbb{B}] \propto V_U/V$ have been introduced:

$$\Delta = f\left([\mathbb{A}][\mathbb{B}]\right), \tag{3.12}$$

where:

$$[\mathbb{A}] = x_b \cdot \frac{T_B}{T_G} \cdot \frac{T_B - T_w}{T_G - T_w} \tag{3.13}$$

$$[\mathbb{B}] = (1 - x_b) \cdot \frac{T_U}{T_G} \cdot \frac{T_U - T_w}{T_G - T_w} \tag{3.14}$$

Bargende concluded after many experiments:

$$\Delta = \left([\mathbb{A}] + [\mathbb{B}]\right)^2 \tag{3.15}$$

The combustion term in neglected because this study is developed on a single-zone thermodynamic model and there is not distinction such as burned and unburned zones.

Han heat transfer coefficient

Han developed a heat transfer correlation to evaluate the instantaneous heat transfer rate specifically for SI engines. The derived expression is:

$$h = 687\, P^{0.75} U(\theta)^{0.75} D^{-0.25} T^{-0.465} \tag{3.16}$$

$$U(\theta) = 0.494\, V_p + 0.73 \times 10^{-6} \left(1.35 P \frac{dV}{d\theta} + V \frac{dP}{d\theta}\right) \tag{3.17}$$

where $U_{(\theta)}$ is representing the average gas velocity at each crank angle and the second term in of the equation represents the turbulence in the cylinder depending on pressure and volume gradients. These terms represent how pressure and volume changes and combustion motion influence to rise the gas motion, thereby the convective heat transfer.

Heywood heat transfer coefficient

The Heywood heat transfer correlation is an empirical model which is applied in internal combustion engines (ICEs). Heywood uses a two term velocity w that adds a combustion induced component to the mean piston speed term.

$$h = 3.26 \cdot B^{-0.2} \cdot P^{0.8} \cdot T^{-0.4} \cdot w^{0.8} \tag{3.18}$$

Eichelberg heat transfer coefficient

The Eichelberg heat transfer correlation is one of the most simplified models for evaluating the convective heat transfer coefficient in ICEs. The basic formula is highlighted below.

$$h = 7.67 \times 10^{-3} \cdot c_m^{1/3} \cdot \sqrt{p \cdot T} \tag{3.19}$$

Combustion model

The duration of combustion is depicted by the energy which is released due to combustion of charge Q_x and can be illustrated below as:

$$\frac{dQ_x}{d\varphi} = Q_t \cdot \frac{dx_b}{d\varphi} \tag{3.20}$$

The parameter Q_t is the total thermal energy of the fuel which is released during the combustion, the full expression is depicted below.

$$Q_t = m_{\text{fuel}} \cdot \text{LHV}_f \tag{3.21}$$

In single-zone thermodynamic modeling, empirical or semi-empirical sub-models are usually used. One of those is the Wiebe function which is applied to estimate the rate of the burned mass (combustion rate). The single or multiple Wiebe function is flexible in accuracy of capturing various combustion patterns. For example, some of these patters are: a simple flame propagation in SI engines and a two stage diesel combustion. The flexibility of Wiebe function makes it an effective approach for modeling a wide range of combustion processes in different type of engines. The Wiebe function which is widely used for approaching the rate of burned fuel rate and its also used in SI engines is depicted below.

$$x_b = 1 - \exp\left(-\alpha \cdot \left(\frac{\varphi - \varphi_0}{\Delta\varphi}\right)^{b+1}\right) \tag{3.22}$$

Where x_b is the mass fraction which is burned, φ is the crank angle, φ_0 is the crank angle at the start of the combustion, $\Delta\varphi$ is the duration of the combustion, b is the shape factor and the parameter α, defines the characteristics or the quality of the combustion. It can be expressed as:

$$\alpha = \ln(1 - x^*) = -6.908 \tag{3.23}$$

Where x^* =0.999, representing the fraction of fuel that is burned at the end of the combustion.

The differential form of Wiebe equation can be expressed as:

$$\frac{dx_b}{d\varphi} = \alpha \cdot \frac{b+1}{\Delta\varphi} \cdot \left(\frac{\varphi - \varphi_0}{\Delta\varphi}\right)^b \cdot (1 - x_b) \tag{3.24}$$

In this study the combustion is modeled with a double (two-stage) Wiebe function. The choice reflects the chamber flow and geometry. The converted diesel engine to a natural gas spark ignition engine has particular geometry (instead of flat head piston, bowl-in head piston is mounted on the engine) which affects substantially the combustion. During compression a big flow from the squish region into the bowl. This interaction with the motion of the piston generates a tumble flow. The combination of these two motions increase the turbulence in the bowl near TDC (Top Dead Center) compared to the squish region. The motion of this flow (a feature characteristic of diesel chamber geometry) divided the combustion event into two stages separated by when and where they occur.

Inside the bowl the flame is relatively thick and advanced quickly. In contrast, in the squish region the flame is thinner and progressed much more slower. Additionally, turbulence is higher in the bowl region and lower in the squish. This is because, the turbulent flame speed is greater in the bowl than in the squish. To account the two separate stages of combustion with the different characteristics for a 0D combustion model, a double Wiebe function is used. Using a double-Wiebe function (one stage for the rapid bowl burn and another for the slower squish burn) yields high accuracy in predicting the combustion process of this converted engine. The standard Wiebe function fails to predict the mass fraction burned for the two stage combustion diesel engines converted to lean natural gas spark ignition, since it was formulated for a one stage burn.

4

Experimental Setup

For the study an 8-cylinder four stroke, turbocharged marine high speed natural gas (NG) lean burn (LB) engine is used. No new experiments were performed in this thesis. All the data were taken campaign reported in [44] measured on the same multi-cylinder marine SI engine. Delivering 500kWe at 1500rpm and a small valve overlap period, key parameters are illustrated in Table. In that study, in cylinder pressure was recorded with uncooled piezoelectric transducers (Kistler 7061C) and charge amplification (Kistler 5064C), with traces pegged to intake pressure using a two-point polytropic compression method. Crank position was measured with a 720-ppr optical encoder (0.5°CA resolution), and at least 400 consecutive cycles were acquired per operating point and ensemble averaged. Boundary-validation signals included manifold pressures and temperatures (K-type thermocouples), natural gas flow (Bronkhorst F-106C1), and exhaust emissions using a HORIBA PG-350 and a Thermo-FID analyzer for methane and total UHC. Test stability was ensured by operating the engine for a minimum of five minutes between operating point transitions while parameters such as exhaust temperature, fuel flow, and emissions were monitored continuously.

The dataset spans 26 steady-state operating points covering load, air-excess ratio (λ), spark timing, and intake-temperature sweeps (maximum generator power limited to 432 kWe by the NG supply. Hence, details are provided because they determine the fidelity of the mass-fraction-burned and heat-release curves used to calibrate and validate the two-stage (bowl and squish) Wiebe function.

Engine type	8-cylinder, turbocharged, lean-burn, 4-stroke
Ignition mode	Spark ignition
Combustion chamber	Flat head and bowl-in piston
Displacement [L]	34.5
Bore $\times$ stroke [mm]	170 $\times$ 190
Rated power/speed [kWe/rpm]	500/1500
Compression ratio [–]	12:1
Number of valves [–]	4
Intake valve opens/closes [°CA aTDC]	337 / -122
Exhaust valve opens/closes [°CA aTDC]	140 / 377

Table 4.1: Engine specifications.

Originally designed as a diesel, the engine was converted to NG SI engine with only limited changes. One of these changes was the alternation of piston's geometry. A hemispherical bowl-in piston crown was introduced for the SI engine. This new design lowered the compression ratio to 12:1. The usage of this piston shape boosted the squish flow and the turbulence near TDC, preserving the diesel design and accelerating the flame development. The multi-cylinder marine SI engine which was used for the study. he main constituents and properties of the natural gas used for this experiment are summarized in Table 4.2.

Property	Value
Methane [Vol. %]	80.8
Ethane [Vol. %]	3.18
Propane [Vol. %]	0.71
Nitrogen [Vol. %]	13.1
CO_2 [Vol. %]	1.69
Density at 25 °C [kg/m^3]	0.77
Lower calorific value [MJ/kg]	38.12
Wobbe-index [MJ/m^3]	39.94
Methane number [–]	83

Table 4.2: Main constituents in the NG and properties.

Figure 4.1: Engine test bench.

5

Results

5.1. Heat Transfer Coefficients and Comparison

In this section, the instantaneous convective heat-transfer coefficient $h(\theta)$ is evaluated within a single zone thermodynamic model for the correlations listed below: Woschni [38], Annand [39], Hohenberg[35], Sitkei [40], Bargende [42],Han [41], Heywood [43]and Eichelberg [36]. Following this assessment, this study aims at comparing the prediction of the convective heat transfer coefficients. Because most correlations were tuned or validated on single cylinder SI engines, notably several were originally developed not just tuned using sophisticated experiments that measured temperature gradients across the cylinder wall. They are assessed here under multi cylinder SI conditions (characteristic engine geometry) using identical boundary conditions and gas properties, as summarized in section 2.4. For each correlation, the crank-angle–resolved coefficient $h(\theta)$ is computed over the cycle, and the resulting profiles are highlighted in section 2.3.2.

The data of in cylinder pressure and temperature traces were used to compute the heat transfer coefficients $h(\vartheta)$. The baseline operating points were: 100kWe, 200kWe, 300kWe, 400kWe and 432kWe. For each operating point, all correlations are run with identical inputs such as: engine's geometry, speed, pressure and trapped mass. This section examines the key characteristics of the heat transfer correlations' profiles, to better understand their differences which is important prior to the selection of the most appropriate for the LBSI engines.

The temporal resolution for the simulation is 11ms , equivalent to Dth 0.1 CA at 1500 rpm. The gas properties $c_p(T)$ (specific heat at constant pressure, $\mathrm{J\,kg^{-1}\,K^{-1}}$), $k(T)$ (thermal conductivity, $\mathrm{W\,m^{-1}\,K^{-1}}$), $\mu(T)$ (dynamic viscosity, Pa s), and $\gamma(T) = c_p/c_v$ (specific–heat ratio, –) are modeled as temperature dependent for a fixed NG composition. This study intends to apply the correlations as developed in their original study, including their empirical constants. All correlations are used to evaluate the $h(\theta)$ in the combustion window, which has been determined experimentally (cite the Applied thermal engineering paper here), subsequently simulating the crank-angle resolved heat transfer $Q_w(\theta)$.

In addition, there is evaluation for five power points, representative of the test campaign at fixed speed n=1500 rpm, holding the remaining inputs identical unless stated. Below are illustrated some of the most important parameters.

Load & Speed		p_{man}	T_{man}	Air flow	Fuel flow	ST
(kW)	(rpm)	(bar(a))	(°C)	(kg/s)	(Nm^3/h)	(°CA)
100	1500	0.703	39.43	0.250	55.23	20
200	1500	1.118	38.82	0.436	83.82	20
300	1500	1.483	38.25	0.601	111.16	20
400	1500	1.858	37.24	0.763	138.99	20
500	1500	1.989	37.03	0.797	148.24	20

Table 5.1: Operating points.

At the operating points summarized in Table 5.1, the crank-angle–dependent convective heat-transfer coefficient $h(\theta)$ was computed using seven widely used correlations within the single-zone methodology of Section 3.1. For each correlation, the crank angle resolved heat transfer coefficient $h(\theta)$ is computed and comparable metrics are derived. The analysis aims to assess the feature: 1) how profile shapes differ over the combustion. First, the 100 kWe load case is presented and discussed. Later in the thesis, the five operating points are compared and discussed. Below the instantaneous heat loss graph is illustrated in figure 5.1, it compares the crank-angle resolved heat transfer as simulated in the various correlations employed.

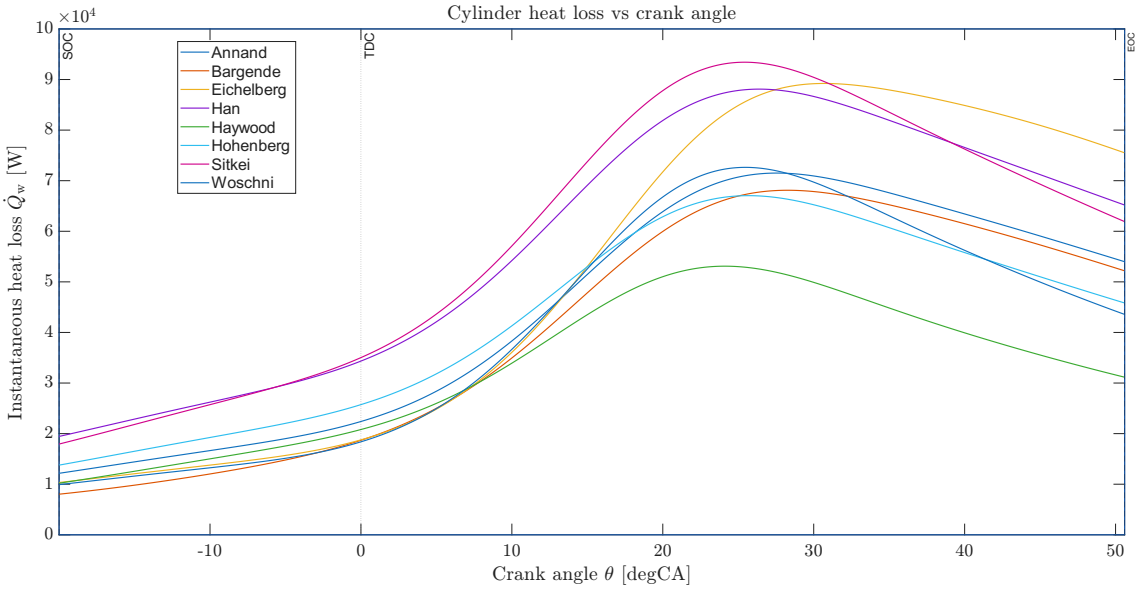

Figure 5.1: Instantaneous heat loss $\dot{Q}_w(\theta)$ vs crank angle at 100kWe, 1500 rpm (SOC–EOC).

The curves of ”Heat loss” gradually increase, peak around TDC with the main heat release and decreases over the early compression. The governing equation of the instantaneous heat loss is given in equation (3.3).

Figure 5.1 shows instantaneous heat loss $Q_w(\theta)$ at 100kWe and 1500 rpm (SOC-EOC). The heat loss rate toward the TDC, peaks near the main heat release phase, and then decreases during early expansion. Across the seven correlations differences appear mainly as magnitude offsets and the steepness of the rise and decrease, while the timing and overall shape remain similar.

The convective heat loss follows the relation in equation (3.3). In this single zone thermodynamic model, the wall temperature T_w is fixed. The in cylinder gas temperature $T_g(\theta)$ comes from the same single zone solution for all cases, and the exposed area $A(\theta)$ is purely geometric (identical across correlations). Consequently, the only term that depends on the chosen correlation is the heat transfer coefficient $h(\theta)$. Thus, any differences observed in the heat-loss curves arise from the heat-transfer coefficient. The comparison is therefore framed in terms of the heat transfer coefficient $h(\theta)$.

As the representative operating point, heat loss increases towards and decreases during early expansion. The overall shapes of the heat-loss curves are similar across models. The main differences are the peak magnitude and the slopes of the rise and decay. This is because the temperature difference and exposed area evolve in the same way for all cases. Only the heat transfer coefficient differs between correlations. For example, correlations with stronger sensitivity to gas velocity or turbulence predict higher heat transfer coefficient h near TDC and therefore higher peak.

As is was observed, across different loads, the magnitude levels of heat transfer increase, but the timing and the shape change in a modest way. Since $\Delta T(\theta)$ and $A(\theta)$ are identical for every correlation, the magnitude and the total shape is determined by how each correlation's $h(\theta)$ responds to the changing thermodynamic state (pressure, temperature) and characteristic velocities. Based on these data, the study focuses on: differences in $h(\theta)$ profile shapes over the combustion and which correlation provides the most credible absolute magnitude and load scaling without any tuning. Figure 5.2 depicts $h(\theta)$. As established above, this is the term that differentiates the correlations. Hence, the detailed comparison uses the $h(\theta)$ curves.

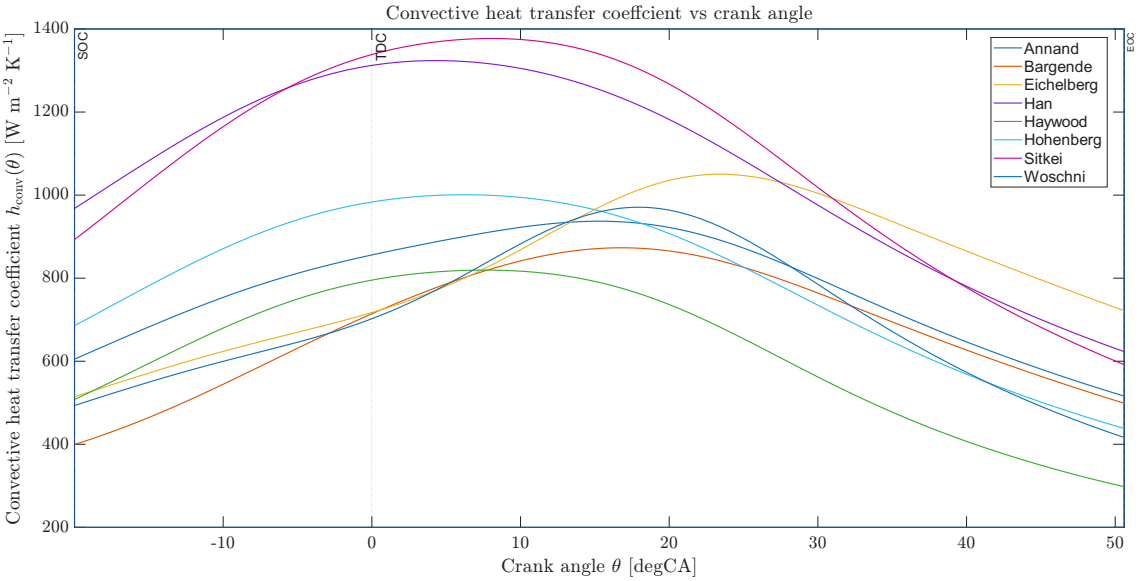

Figure 5.2: Convective heat-transfer coefficient $h(\theta)$ vs crank angle at 100 kWe, 1500 rpm.

Figure 5.2 illustrates and compares empirical in cylinder convective heat transfer coefficients during the combustion phase at 100kWe and 1500 rpm. The profiles across different models differ because each correlation treats gas motion, geometry, and gas-property temperature effects differently, and their constants were fitted on different testbed engines. All correlations rise through late compression, reach a maximum shortly after TDC, and then decrease during expansion. The peak crank angle varies by model: early peaks around 5–10° ATDC (e.g., Hohenberg, Han, Sitkei, Heywood), a middle group near 12–18° after the point of TDC (Woschni, Annand, Bargende), and a later peak around 18–25° after TDC (Eichelberg). Sitkei forms the upper envelope.

Specifically, the heat transfer coefficient of Hohenberg peaks early and forms a broad plateau around TDC because it multiplies a strong pressure term with instantaneous volume-chamber size ($V^{-0.06}$), so because this term is negative and volume is shrinking toward the TDC the h is amplified around TDC. Beyond that point, as piston expands and in-cylinder volume increases, convective heat transfer starts decreasing. The pressure parameter ($p^{0.8}$) contributes considerably to the ”early lift” of the curves, since the moment that pressure starts from 12 bar. A small combustion turbulence offset (constant, C_2) in the velocity factor further boosts the rise as soon as the combustion begins. The constant (C_1) reflects on ”swirl” and it raises the whole curve without changing the peak. It raises the entire Hohenberg curve (and the TDC plateau) proportionally, with no effect on the timing or breadth of the peak. The negative temperature exponent ($T^{-0.4}$) pulls down the curve smoothly as gas gets hotter and to the point of TDC. The Hohenberg correlation was derived and calibrated on direct-injection, obtained from multi engine DI datasets. As highlighted by the study of Hohenberg [45], SI engines have distinctly different pressure and gas velocity conditions than diesel engines, requiring a refitting of the correlation in case of its application to SI engines.

The heat transfer correlation of Han rises directly to combustion-driven gas motion, not geometry. The gas velocity $U(\theta)$ includes a piston driven flow $(C_2 V_p)$ plus a combustion induced term proportional to $\big(1.35\,p\,dV + V\,dp\big]\big)$. The Wiebe heat release trace increases before p_{max} and over many crank angle degrees, so the combustion term in $U(\theta)$ turns on early and stays high for a wide range of crank angles. The coefficient $h(\theta)$ follows that, illustrating an early start and a wide tip. The curve rides on a high baseline set by the mean flow term of $U(\theta)$ which is $(C_2 V_p)$. The combustion contribution gives a medium bump on top, so $U(\theta)$ and $h(\theta)$ stay at high levels even away from the peak of heat release. The result is a wide and rounded plateau. Therefore, smoothing the pressure signal rounds off the sharp changes ($\frac{dp}{d\theta}$), so the peak looks flatter and wider. The combustion term jumps, which makes $U(\theta)$ and the heat transfer coefficient peak earlier than the pressure maximum. The constant C_1 represents the chamber air-motion differences (swirl and bowl shape) and it is a pure scale factor raising the entire curve without changing the peak or the width. The constant C_2 represents the combustion induced turbulence (piston driven velocity) and again its lifting up the curve during combustion without affecting the shift or the peak. The constant C_3 represents how strongly apparent heat release drives the in cylinder turbulence. Han’s moderate temperature term damping does not force a fast decrease beyond TDC. Han at [41] worked on SI engine powered with gasoline and compared predictions and measurements at relatively high speed range from 2000 to 3000 rpm.

In the Sitkei correlation, the convective heat transfer coefficient is predicted to reach the largest maximum of the combustion phase right after the TDC. This behavior is driven by the use of an equivalent crank angle depended diameter

$$d_e = \frac{4V}{A}$$

. This dimeter is minimized near TDC as the liner area and the clearance volume are small, while the cylinder pressure is high. This combination produces a strong rise to a dominant peak to the heat transfer coefficient. As the piston descends early expansion, V and A_{liner} increase, d_e grows and pressure falls, so the heat transfer coefficient decays. The resulting curve is characterized by a maximum near TDC followed by a rapid decrease.

The Heywood heat transfer correlation peaks relatively early because near TDC the pressure term $p^{0.8}$ is rising and the velocity boost turns on as soon as combustion makes $p > p_m$. At the same time the factor $\frac{V_d\,T_r}{p\,V}$ is greater at smaller volumes, so the combustion term in w jumps before the

pressure maximum. The profile is broad because a constant term $C_1\, S_\mathrm{p}$ is present throughout the cycle, and the pressure boost term $p - p_m$ stays positive, keeping the curve elevated for longer. The medium negative temperature exponent ($h(\theta)$) decreases gradually through expansion. The curve's overall shape is smooth with a rounded hump (since the moment that there is not instantaneous geometry and no turbulence spike). In terms of sensitivities, pressure factor $p^{0.8}$ has the strongest influence in lifting. The geometric parameter of $B^{-0.2}$ has a weak influence in the curve's shape. A faster temperature rise represented by T_g^{-n} with $n = 0.55$ results in a smoother post TDC decay. Further smoothing of $p(\theta)$ or of the motored reference $p_m(\theta)$ flattens and broadens the top. As a result, the top of the curve appears wide and low, achieving the lowest peak among all heat transfer correlations. Accordingly, the heat transfer coefficient profile illustrates a broad, and attains the lowest peak among the plotted correlations. The instantaneous Haywood correlation was developed on a high speed DI diesel engine. At [11] it is mentioned that, the model tracks the burn reasonably but tends to miss on gas exchange.

The correlations of Han, Hohenberg, and Haywood peak early for different reasons as they are highlighted already. Among the three, Han predicts the biggest peak for heat transfer coefficients. Hohenberg is intermediate, and Haywood is the lowest and broadest. This is a reflection of Han's combustion term (velocity) and the larger scaling constants. Sitkei at [40] highlighted that the correlation is developed for diesel engine.

During compression the heat transfer coefficient of Annand increases as piston gets closer to TDC. This can be attributed to the rise in density $\rho \sim \frac{p}{RT}$. Another reason for the curve's rise is the increase of the thermal conductivity $k(T)$ as the gas getting hotter. The opposing effect of viscosity increasing with temperature (T) is "weaker" than the rise from density. As a result, the Reynolds number $Re^{0.71}$ elevates and further boosts $h(\theta)$. The peak of the curve appears after TDC, because as the velocity becomes zero at this point. Right after TDC, the piston accelerates while the pressure and the density remain high. This gives a maximum value for Re, thereby $h(\theta)$. At the expansion phase the pressure drops (turbulence decreases as well) and dominates the viscosity reduction. This reduces Re and subsequently $h(\theta)$ resulting in a smooth and asymmetric heat transfer profile with a late peak. Published engine heat transfer data primarily Elser's open chamber diesel measurements (∼300 rpm) reanalyzed by Annand [39]. The Annand-type correlation $\mathrm{Nu} = a\,\mathrm{Re}^A \mathrm{Pr}^B$ was fitted, with the bore used as the length scale and the mean piston speed used as the velocity scale (an optional radiation term was included). The constants were noted to be engine specific. This is relevant here because the datasets on which these correlations were developed differ from LBSI engine in geometry, combustion mode, and operating conditions.

The Eichelberg heat transfer correlation[36] forms a curve which is broad with a steeper bump after TDC. The curve is driven almost totally by the product of the in cylinder pressure and temperature while mean gas piston speed term $(V_{mp})^{(1/3)}$ remains constant over the cycle. Through late compression, both p and T increase sharply as the gas is heated, so $\frac{p}{T}$ rises steadily, therefore h rises as well. After TDC, rapid heat release keeps increasing T while p is near to its maximum value. This is the point where $p \cdot T$ reaches its maximum, so the curve peaks after the point of TDC. As expansion proceeds p drops quickly, even if temperature remains high briefly, the falling p dominates the product and h decreases smoothly. The slope is steeper as long the pressure and the temperature are increasing and smoother when pressure decreases and temperature stays high. The correlation was based on period reciprocating diesel engines (single cylinder). Again it is essential to be tuned for better accuracy for different type of engines.

The Bargende curve rises gradually during the late compression, peaks fairly late and then decreases smoothly. The shape follows the balance in the correlation, with the strong factors of pressure and gas motion ($p^{(0.78)}$, $w^{(0.78)}$) pushing h up. On the contrary, the negative temperature sensitivity $T^{(0.47)}$ and the weak volume term rise. Near the point of TDC the effective gas velocity w is small because the instantaneous piston speed is small, even with high pressure, rising temperature limits the increase. Just after TDC, piston speed (w) rises rapidly while pressure is still relatively high, so $p^{(0.78)}$, $w^{(0.78)}$ overwhelms the damping and produces a late broad maximum. Further into expansion, pressure falls, volume grows and w levels off. Temperature is still high, and because the model uses $T^{0.477}$, a higher temperature gives a smaller total result. With w no longer increasing, there is nothing to balance these effects, so the curve of h decreases gradually, creating a long smooth extension.

The Woschni curve increases smoothly during compression, $p^{(0.75)}$ rises while the negative temperature term $T^{(0.62)}$ damps the rise of curve (h). The term of gas velocity is driven mainly by the mean piston and swirl components, which do not change much near TDC. After the point of TDC the Woschni firing term, which is proportional to $p - p_{mot}$ switches on quickly. Pressure is still high, so the value of $p^{(0.75)}w^{(0.786)}$ increases rapidly, creating sharp peak after TDC. As combustion ends, $p - p_{mot}$ falls away so the velocity term decreases, the pressure also falls and the term of temperature $T^{(0.62)}$ keeps decreasing, h falls gradually through expansion. The constant C_3 which is the firing gain and is multiplied with the combustion velocity term, assists in the rapid rise of h. A big value of C_3 means that the moment $p - p_{mot}$ increases, w rises faster. If C_3 is smaller, the velocity would grow more gradually. The term of swirl mainly lifts the values near TDC but it does not create any the spike. The spike is created by the fast ”on-off” of the firing term. Woschni's correlation initially applied on a Diesel engine. It is highlighted that the correlation is ”universal” usable if different constants are used for different engine designs.

Across the eight correlations at 100 kWe and 1500 rpm, all of the heat transfer coefficients h rise during later compression, peaking after the point of TDC, then declining during expansion, but they are different in height of peak, timing and shape because each treats gas motion and thermodynamic properties differently. In addition the constants differ because the correlations were developed and calibrated on different engine types, each with distinct geometry, combustion mode, and operating conditions. Sitkei's correlations has the highest peak. The earliest peaks are Han and Hohenberg. Han peaks early because its velocity term includes a combustion driven term ($1.35\,p\,dV + V\,dp$), that turns on before p_{max}. Hohenberg peaks early after TDC forming a wide plateu. Is driven by ($p^{0.8}V^{-0.06}$) and medium $T^{-0.4}$ damping. Haywood peaks early like Han and Hohenberg but gives the lowest values compared to all of the heat transfer correlations, yet the peak is wide and not sharp. After them, Annand climbs smoothly and asymmetrically to a its maximum value just after TDC. Immediately past TDC the piston speed term w rises quickly while pressure (and thus density) is still high, so the Reynolds (Re) number peaks shortly after TDC and . The heat transfer coefficient of Bargende is built more slowly and peaks almost at the same time with Annand (it is peaking a bit later), creating a wide bump as pressure and gas motion balance the temperature term. Woschni shows the sharpest and narrowest top, its firing term creates a characteristic spike. Eichelberg is last to peak, raising a tall peak because the term pT continues to grow into early expansion. Temperature increases and at the same time pressure remains high, before the pressure drop finally dominates and the curve decreases.

Heat transfer correlation	Peak crank angle (°CA)
Han	3-5
Hohenberg	4-7
Sitkei	7-9
Heywood	7-9
Annand	14-18
Woschni	15-18
Bargende	15-19
Eichelberg	22-24

Building on the 100 kWe analysis, the following graphs present $h(\theta)$ for 200, 300, 400, and 432 kW at 1500 rpm, computed with the same settings(constants, pressures). For each load, peak magnitude, peak crank angle relative to TDC, and the general shapes of the models are depicted. With increasing load, peaks are generally observed to increase and to shift toward the point of TDC. A concise comparison of the heat transfer coefficients is provided for every load which is applied.

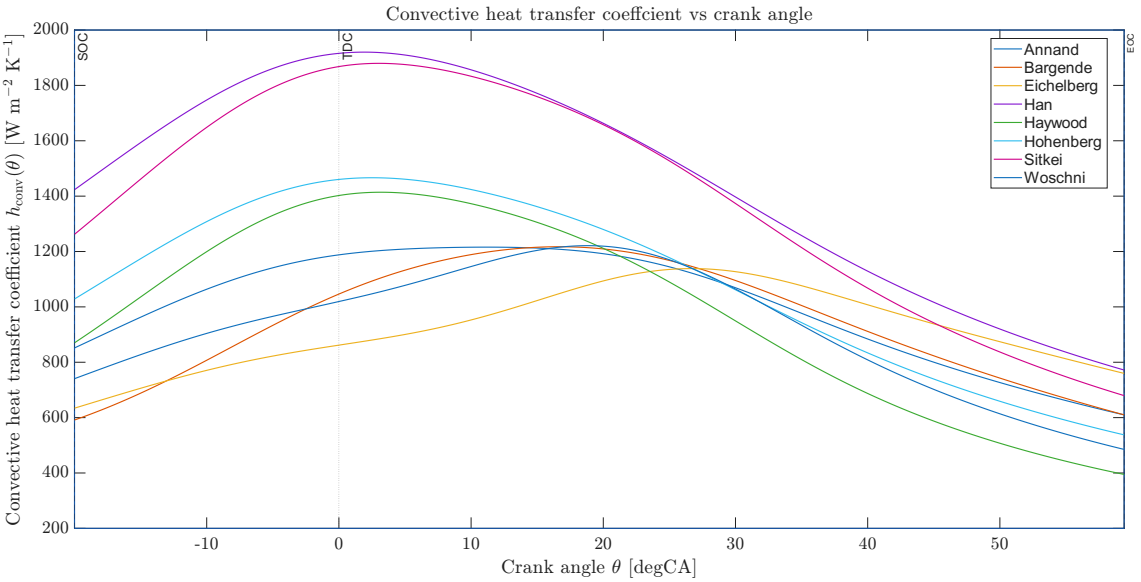

Figure 5.3: Convective heat-transfer coefficient $h(\theta)$ vs crank angle at 200 kWe, 1500 rpm.

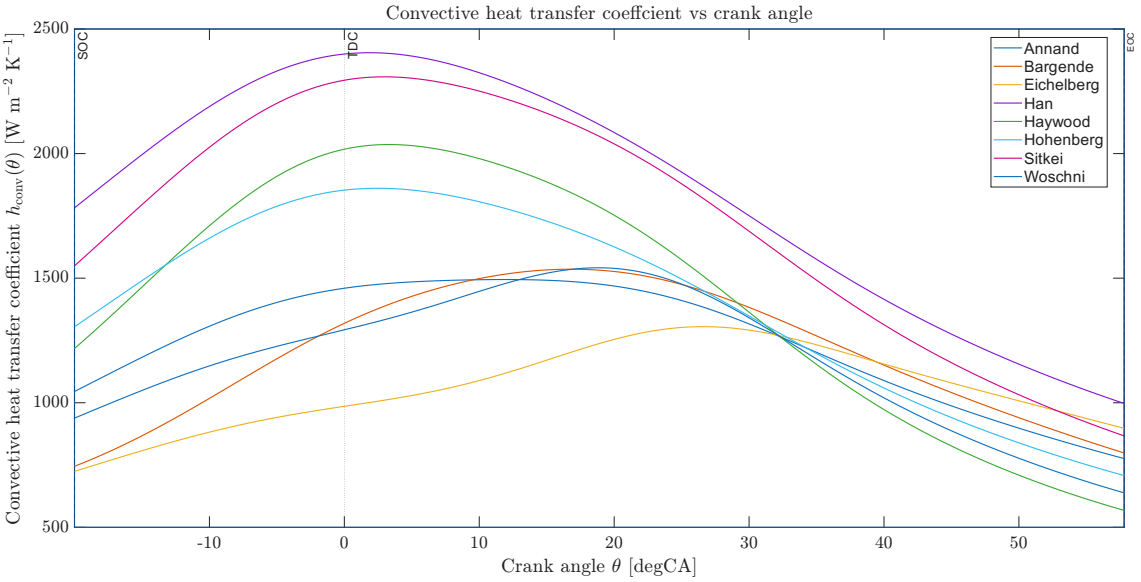

Figure 5.4: Convective heat-transfer coefficient $h(\theta)$ vs crank angle at 300 kW, 1500 rpm.

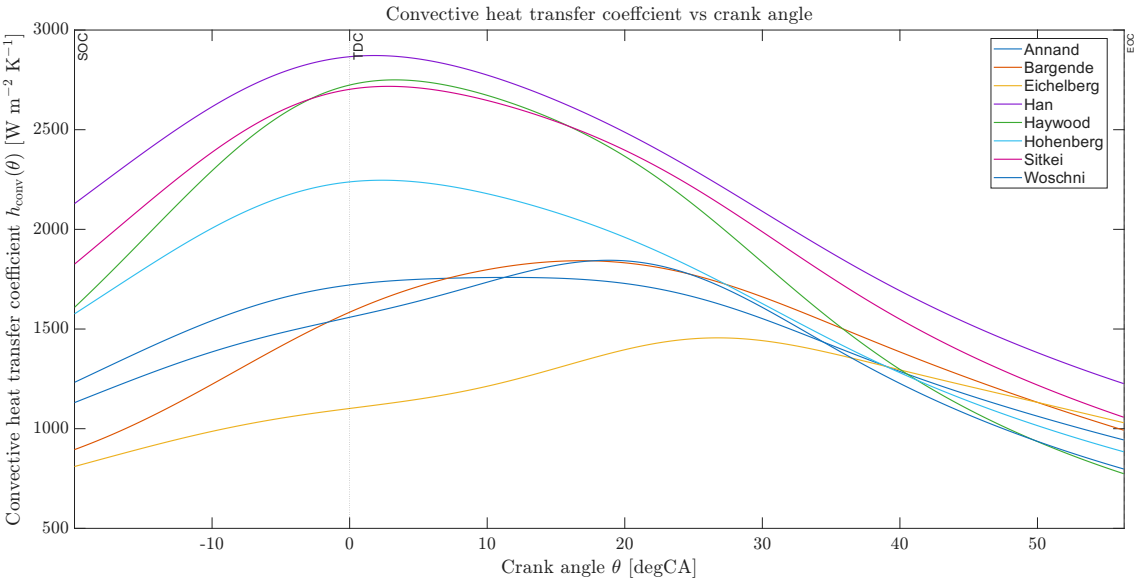

Figure 5.5: Convective heat-transfer coefficient $h(\theta)$ vs crank angle at 400 kW, 1500 rpm.

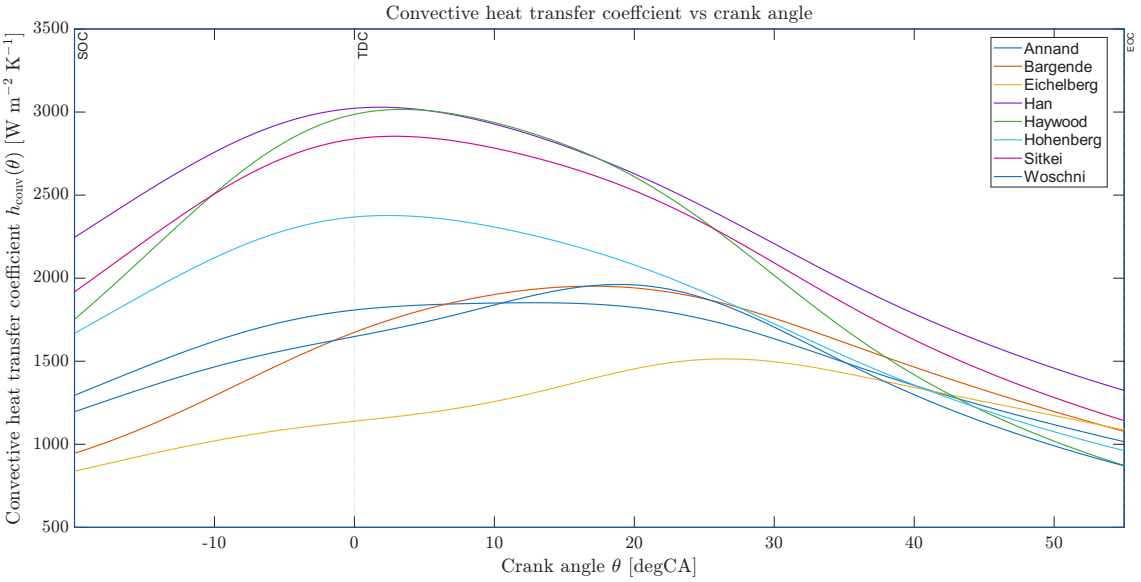

Figure 5.6: Convective heat-transfer coefficient $h(\theta)$ vs crank angle at 432 kW, 1500 rpm.

A cross load comparison of for the loads of 200-432 kW at 1500 rpm is presented. With increasing load, the curves are generally observed to rise and to shift towards the point of TDC.

The peaks that occur a few °CA after TDC at 100 kW move closer to TDC at higher loads. The characteristic shapes remain recognizable. For the load of 200kWe the curves of Han and, Sitkei, Hohenberg and Heywood have the earliest increases to the maximum points. With load increased, peak pressure and $dp/d\theta$ rise, so correlations that are sensitive to pressure or combustion driven velocity such as Han, Hohenberg, Woschni show the biggest increase near TDC. For example, Woschni's correlation includes a firing term $(p - p_{mot})$ which produces sharper peak, overtaking smoother models. At 200 kW, Han reaches the highest peak, overtaking Sitkei. The change is due to Han's explicit term which is related to the combustion factor. The factor, $\left(1.35\,p\,dV + V\,dp\right)$ is rising and strengthens with the higher pressure rise at this load, creating an steeper and earlier peak (compared to the load of 100kWe). Sitkei rises more uniformly, retaining a broad high level, closer to the point of TDC, but a slightly lower than Han's. The correlation of Annand changes are moderate because the temperature parameter and the viscosity term are increased, slowing down

the Re factor, so the growth of the coefficient is smoother. The models (Bargende, Eichelberg) which are peaking later during the expansion, kept rising because of their key parameters pT and $p^{0.78}$ and $w^{0.78}$, staying relatively high. At 200 kW the Haywood peak is noticed to move from the lowest rise to a higher position. The increase is explained by the stronger pressure parameter which is emphasized in Heywood.

For the higher loads of 300, 400 and 432kWe, the form of the shapes are retained while the amplitudes rise for all heat transfer correlations. The maximum peaks are closer to the point of TDC (just like for the laod of 200kWe). The earliest increases continue to illustrated by Han, Sitkei, Hohenberg and Heywood, heaving their peaks near TDC. As long the load increases their amplitude rises, reflecting to rise of the pressure and the combustion terms. Woschni's peak remains the narrowest among the models. However, it is noticeably broader than in the 100 kWe load, so for the rest of the loads the curve shows a wide peak. Annand maintains a gradual increase, reaching the maximum peak after TDC. Its rise with load is smooth because the temperature effects slow down the Reynolds number increase (influence). The heat transfer models of Bargende and Eichelberg remain late and broad. Specifically the model of Eichelberg is the last to peak because of the pT term remains high into early expansion before the pressure drop dominates. The dominant trends are a uniform increase in amplitude, the early maximum peaks move toward the point of TDC, and some of the peaks broaden (Woschni). The expansion side does not generally become steeper.

5.2. Validation and Sensitivity Analyses

5.2.1. Validation against experiments

Experimental validation is essential for assessing simulating models and ensure their reliability and accuracy. In this context, the present chapter evaluates the employed heat transfer models, discussed in Chapter 5, by comparing their simulating results with experimental data obtained from an NG-fueled LBSI engine. As there are limitations in quantifying instantaneous heat transfer in these multi-cylinder engine testbeds which rely on in-cylinder pressure,direct comparison of crank angle resolved heat transfer is infeasible. Cumulative heat transfer, however, as simulated by the applied models, can be meaningfully compared to the overall heat transfer estimated from engine energy balance calculations in the experimental studies [44]. Consequently, this chapter presents a comparative analysis of predicted cumulative heat transfer at the end of combustion EOC across several operating points relative to experimentally derived values for validation.

The criteria used to evaluate each heat transfer correlation are stated below:

- Agreement with experiment, quantified per load by the relative error in (5.3) and summarized across loads by mean absolute percentage error (MAPE) in (5.4).
- Literature suitability, whereby greater weight is given to correlations which developed and validated for SI engines.
- A quality-versus-complexity assessment is used to capture required inputs.

For each operating case, the heat transfer is simulated using the various convective coefficient correlations $h(\theta)$. The instantaneous convective heat loss is obtained by equation (3.3). This cumulative heat loss Q_{conv} is the integral of the crank angle resolved heat transfer between SOC to EOC.

Accordingly, the cumulative convective heat loss is written as:

$$Q_{\mathrm{conv}} = \frac{1}{6N} \int_{\theta_{\mathrm{min}}}^{\theta_{\mathrm{max}}} Q(\theta)\, d\theta. \tag{5.1}$$

Equation 6.1 represents the energy lost (convective heat loss) in the cylinder during combustion, expressed in joules (J).

The convective heat loss fraction on a fuel energy basis is:

$$f_{\mathrm{pred}} = \frac{Q_{\mathrm{conv}}}{m_f \,\mathrm{LHV}} = \frac{1}{6N\, m_f \,\mathrm{LHV}} \int_{\theta_{\mathrm{min}}}^{\theta_{\mathrm{max}}} Q(\theta)\, d\theta. \tag{5.2}$$

The denominator $m_f \cdot \mathrm{LHV}$ is the input energy of the charge, obtained by multiplying the injected fuel mass by its lower heating value. The ratio of f_{pred} is a dimensionless fraction that quantifies the portion of the fuel energy lost by heat transfer. The operating cases are defined by the load. The SOC-EOC limits used in the experiment were adopted for all comparisons. The experimentally reported heat transfer loss percentages were extracted for five load points: 100kWe, 200kWe, 300kWe, 400kWe and 432kWe. These values are treated as a reference and are used for comparison with the model results. For each load the cumulative heat loss was captured as in equation (5.1), and the corresponding is calculated from the equation (5.2). Therefore, for each load and each correlation, the predicted fraction of heat loss was compared directly with the experimental fraction of heat loss. The same fuel energy basis ($m_f \cdot LHV$) was used as in the experiment and simulation.

Perfect agreement among heat transfer correlations is not to be expected, because the correlations are empirical, calibrated on different datasets and assumptions. Differences in assumptions introduce deviations when applied here. For example, Woschni was developed from diesel engine measurements and focuses on pressure driven characteristic velocity, which can behave differently under LBSI operation. Annand's correlation was originally formulated for diesel engines with consideration of radiation effects, while it was subsequently adapted and used for SI engines. Hohenberg's correlation was derived and calibrated using direct injection diesel engine. As highlighted by the study of Hohenberg, SI engines exhibit distinctly different pressure and gas velocity conditions compared to diesel engines, requiring for refitting of this correlation when applied to SI engines. Han's correlation and its empirical coefficients were developed and validated specifically for SI engines. The Sitkei–Ramanaiah and Heywood correlations, on the other hand, were developed for diesel engines and the test set up used a single cylinder diesel engine. Eichelberg is an early, correlation commonly used in diesel contexts. Bargende's correlation terms initially required multi-zone quantities (average kinetic energy, temperature of unburned zone) which were neglected, and the expression was adjusted into a single zone. This formulation was developed for SI engines within a multi-zone (two-zone) framework. All correlations were examined in their original published form, without tuning or refitting.

Because Han's correlation was developed and validated initially for SI engines and is used in this thesis in its original (untuned) form, closer agreement with the experimental trend in convective heat loss fraction would be expected than for diesel derived correlations. Bargende's formulation is also SI-oriented, but its original multi-zone terms were reduced to a single-zone, so its trend fidelity may be weaker. On this basis, the predicted and experimental convective heat-loss fractions for the five loads are presented in the table below.

Correlations & Experiment	100kWe	200kWe	300kWe	400kWe	432kWe
Experimental	19.34%	16.05%	14.34%	12.82%	12.08%
Woschni	6.53%	8.20%	9.85%	11.41%	11.88%
Annand	7.01%	8.89%	10.39%	11.79%	12.15%
Hohenberg	6.81%	9.09%	10.98%	12.79%	13.30%
Han	9.28%	12.59%	14.43%	16.43%	17.08%
Sitkei	9.46%	11.49%	13.29%	15.68%	16.42%
Heywood	5.25%	7.96%	10.84%	14.05%	15.19%
Eichelberg	8.13%	9.05%	9.81%	10.5%	10.61%
Bargende	6.48%	8.79%	10.53%	12.17%	12.70%

Table 5.2: Convective heat-loss fractions by load: experiment vs. correlations.

The experimental fraction of fuel energy lost to heat transfer decreases as the engine load increases. This occurs because the fuel energy per cycle grows at a higher rate relative to the increase in heat losses through the cylinder walls. The combustion is completed within a similar crank-angle window and the chamber surface area is fixed, so the time window for heat rejection does not scale with the added fuel. At higher loads, the coolant temperatures increase, reducing the average gas wall temperature difference during most of the expansion phase. As a result, more energy is released per cycle but Q_{conv} grows less rapidly than $m_f\,\mathrm{LHV}$, so the measured ratio $Q_{\mathrm{conv}}/(m_f\,\mathrm{LHV})$ decreases with load.

In contrast to the measurements, the simulations produced a consistent increasing trend with load. In the simulations, an increase of the convective heat loss fraction with load is obtained because the correlations make the heat transfer coefficient h rise with pressure, temperature and velocity as the load increases. At the same time, it is assumed that the temperature of the wall is fixed. With these assumptions, the gas wall temperature difference is not reduced at higher load. Consequently, Q_{conv} grows faster in the model than it does in the experiment and the prescribed fraction $Q_{\mathrm{conv}}/(m_f\,\cdot\mathrm{LHV})$ increases with load.

To quantify these observations, the differences across different load conditions are evaluated between the simulated and experimentally-estimated heat transfer. Specifically, for each load (L_i), the mean and the relative error were computed as the difference between the model and experiment. Here, f_{pred} and f_{exp} represent the convective heat-loss fractions. Relative error ε is defined as below.

$$\varepsilon = \frac{f_{\mathsf{pred}} - f_{\mathsf{exp}}}{f_{\mathsf{exp}}} \times 100\%, \tag{5.3}$$

Using the definition in (5.3), the relative errors for each correlation and load are reported in Table 5.3.

Correlation	100kWe	200kWe	300kWe	400kWe	432kWe
Woschni	-66.19	-48.88	-31.29	-10.99	-1.66
Annand	-65.31	-45.84	-28.31	-8.32	0.59
Han	-51.92	-21.52	0.63	28.11	41.30
Heywood	-72.87	-50.41	-24.42	9.60	25.76
Eichelberg	-57.98	-43.63	-31.61	-18.11	-12.18
Bargende	-66.94	-45.53	-26.75	-5.11	5.17
Sitkei	-50.90	-28.30	-7.29	22.22	35.87
Hohenberg	-66.15	-44.90	-24.27	-0.24	10.47

Table 5.3: Relative error (%) by correlation and load ($\varepsilon = \frac{f_{\mathrm{pred}} - f_{\mathrm{exp}}}{f_{\mathrm{exp}}} \times 100\%$).

Negative values indicate under-prediction and positive values indicate over-prediction. At the lowest load (100 kWe) all correlations under-predict strongly. As load increases, several correlations cross to over-prediction. Han's correlation shows the steepest shift to over-prediction at high loads. Overall, accuracy generally improves with load for most correlations, but several begin to over-estimate at the highest operating point. To summarize overall accuracy with a single value per correlation, the mean absolute percentage error (MAPE) is employed. MAPE is defined as the average of the absolute relative errors across the five loads and is expressed as a percentage.

$$\mathrm{MAPE} = \frac{1}{n}\sum_{j=1}^{n} |\varepsilon_j| \quad (\%). \tag{5.4}$$

Based on equation (5.4), the mean absolute percentage errors for all correlations for the five operating points are reported in Table 5.4. The results indicate the average percentage deviation between prediction and experiment.

Correlation	MAPE(%)
Woschni	31.8
Annand	29.7
Hohenberg	29.4
Han	28.7
Sitkei	28.9
Heywood	36.6
Eichelberg	32.7
Bargende	29.9

Table 5.4: MAPE across five operating points (%)

In selecting the convective heat-loss correlation for the remainder of this study, the formulation of Han was adopted. Although the correlation of Sitkei attains a MAPE comparable to Han (28.9% vs 28.7%), the difference is very small. By contrast the correlation of Han meets two decisive criteria. First, in terms of accuracy, Han achieved the lowest MAPE based on relative error over the SOC-EOC window. Second, from a literature standpoint, Han was developed and validated for SI operation, whereas Sitkei's correlation was developed on diesel applications. While the correlation of Han introduces additional implementation effort through derivative terms ($\frac{dV}{d\theta}$, $\frac{dP}{d\theta}$) this complexity was controlled by smoothing the pressure trace prior to differentiation and did not pose stability issues in the simulations. On the other hand, Sitkei is simpler to implement because it avoids derivative terms and requires fewer signal processing steps. Weighting these aspects, Han's correlation satisfies two of the three criteria (accuracy and literature fit), with Sitkei winning only the simplicity. Given the negligible MAPE gap and the stronger support in the literature for SI operation, the added complexity is acceptable, and the Han correlation is selected as the most applicable for this study.

5.2.2. Sensitivity Analysis

Sensitivity analysis is performed to quantify how uncertainty or variation in model inputs propagates to model outputs, and to rank which inputs exert the greatest influence. In this way, model robustness is assessed, possible nonlinearities or interactions are revealed, and uncertainty bands for key outputs are established. The results are used to prioritize calibration and measurement effort, to focus data collection on the most influential parameters, and to justify either model simplifications or added complexity. This section examines how the Han heat transfer correlation [41] affects the results by varying its calibrated constants (C_1, C_2, C_3, m). As these correlations were developed on an empirical basis, it is necessary to assess the sensitivity of the simulated heat transfer to their empirical parameters. To this end, an uncertainty range was assigned to the Han empirical parameters. Parameter uncertainties were specified by modeling judgment. Distributions were chosen to reflect modeling judgment rather than literature constraints. The parameters were treated as independent, so their uncertainties were specified separately. The resulting variability in the heat-loss signal over SOC-EOC was propagated through the model by random sampling. Uncertainty was propagated by Monte Carlo sampling (N=1500): for each draw, a parameter set was sampled, the heat-loss signal was computed. Also, the wall temperature T_w was treated as constant.

The uncertain inputs used for Monte Carlo sampling are summarized in Table for each parameter. The Normal mean (μ) and standard deviation (σ) were specified.

Parameter	**Distribution**	$\boldsymbol{\mu}$	$\boldsymbol{\sigma}$	**Notes**
m	Normal	$\mu_m = 0.75$	$\sigma_m = 0.0433$	exponent in h
C_1	Normal	$\mu_{C_1} = 687$	$\sigma_{C_1} = 39.6639$	scaling of h
C_2	Normal	$\mu_{C_2} = 0.494$	$\sigma_{C_2} = 0.0285$	multiplies V_p
C_3	Normal	$\mu_{C_3} = 7.3e-07$	$\sigma_{C_3} = 4.2146e-08$	multiplies $\kappa p\,\mathrm{d}V + V\,\mathrm{d}p$

Table 5.5: Normal input distributions used for Monte Carlo sampling.

The resulting cycle heat-loss signal was recorded. The distribution of these samples outcomes is summarized by the histogram in Fig. 6.1.

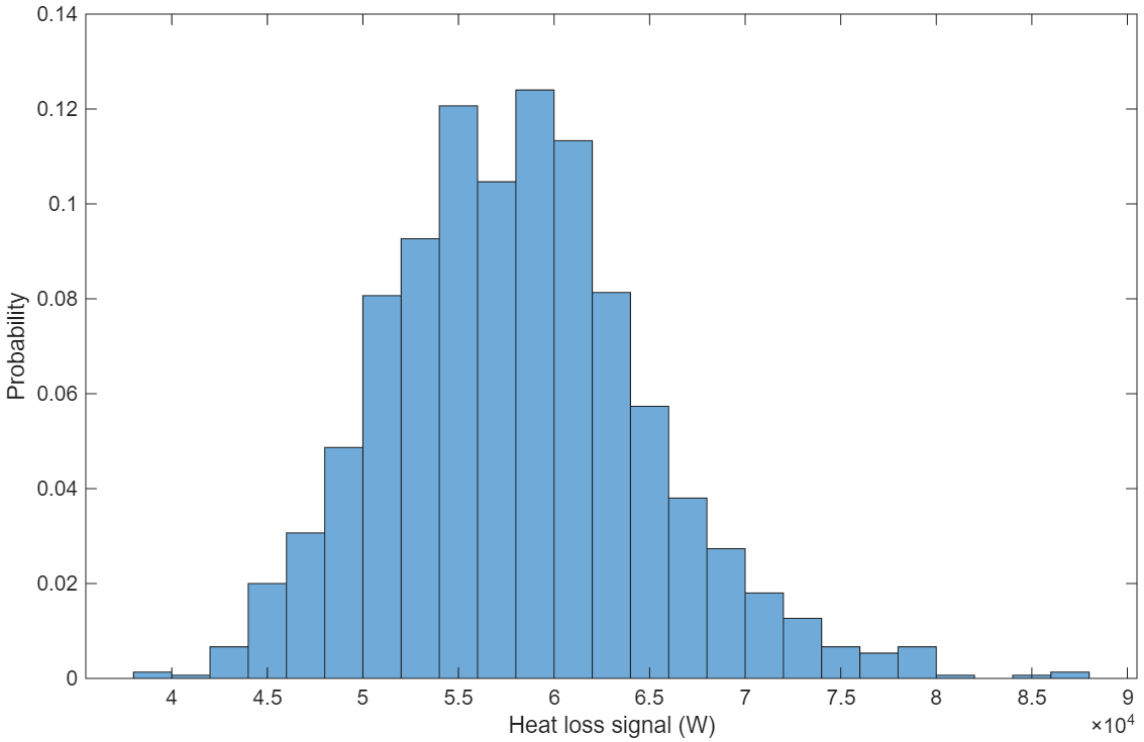

Figure 5.7: Histogram of the in-cylinder heat-loss signal (probability normalization)

The Monte-Carlo distribution of the heat-loss signal is approximately normal but exhibits mild positive skew: most realizations cluster near the central value, with a modestly longer upper tail. This suggests that parameter perturbations around the nominal Han settings produce near linear effects on the output over most of the range, with slightly larger deviations on the high side. Specifically, The Monte-Carlo distribution of the heat-loss signal is centered at 5.81×10^4 with a standard deviation of 6.87×10^3. A few high-end realizations are observed and are attributable to concurrent upper-range draws of the most influential constants.

The sample size was limited to N=1500 due to hardware constraints. For larger number of samples, the computing environment became unresponsive and runs could not be completed. Running statistics of the predicted heat-loss fractions were observed to have stabilized at this run size, indicating that the principal conclusions are insensitive to additional draws. A larger number of samples would primarily reduce Monte-Carlo sampling variability (the histogram would appear smoother) but the underlying distribution and the reported conclusions would be unchanged.

Parameter influence is visualized by scatter plots (Figure 6.2) of the predicted heat-loss signal versus each sampled Han constant, each point corresponds to one of the N=1500 Monte-Carlo draws.

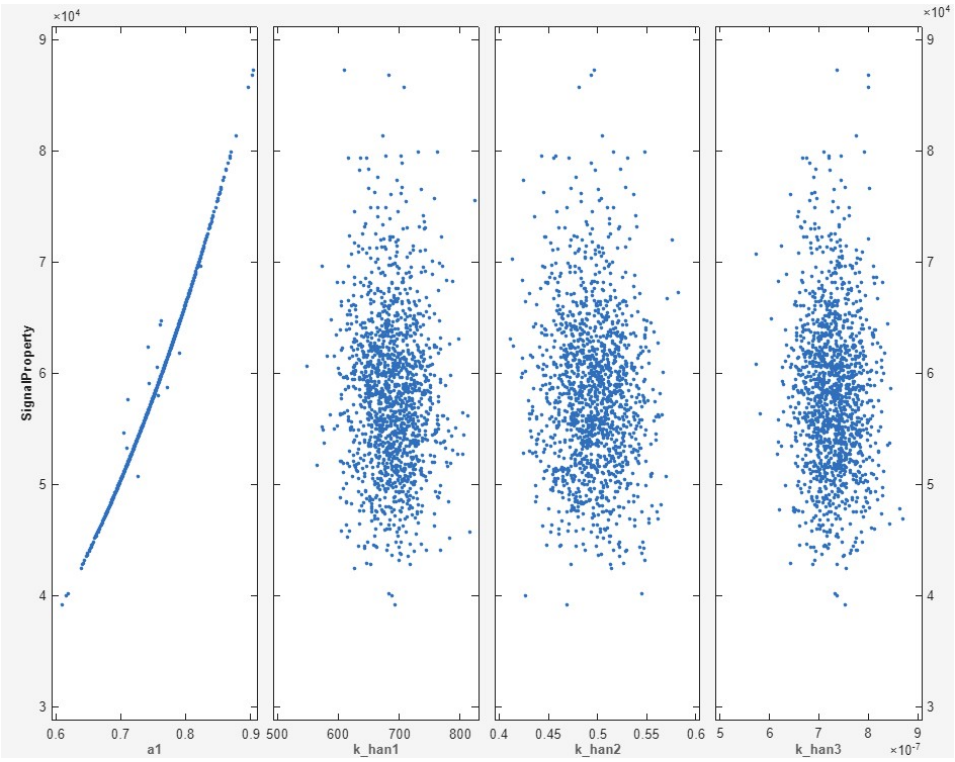

Figure 5.8: Scatter plot

Overall uncertainty is primarily driven by α_1. An almost linear increase of the heat loss signal with α_1 is observed, whereas no meaningful trend is detected for k_{han1},k_{han2},k_{han3} within the tested ranges. Because the parameters were sampled independently the observed effect can be attributed to itself rather than to co-variation. Accordingly, if the uncertainty in α_1 were halved, the spread of heat-loss results would be expected to shrink by roughly the same proportion. By contrast, tightening the uncertainties of k_{han1},k_{han2},k_{han3} would yield negligible changes in the output. The near linear behavior around the nominal also suggests that a single parameter calibration focused on α_1 would capture most of the attainable improvement, with interaction effects not evident over the examined ranges.

6

Conclusion and Recommendation

6.1. Conclusion

This thesis evaluated which in-cylinder convective heat transfer correlation is most suitable for a lean burn spark-ignition (LBSI) marine engine operating on natural gas. A comprehensive literature review was coupled with implementation of several established correlations in a single-zone simulation, comparison without tuning across five loads, and validation against experimentally derived heat-loss fractions over the start of combustion to end of combustion (SOC–EOC) window. On this basis, the most suitable correlation for the present engine and operating range was identified. A brief synthesis of the load-dependent heat-transfer behavior is provided next, as it frames the subsequent validation and selection. As load increases, peak heat-transfer levels rise and the maxima shift closer to top dead center (TDC), while the characteristic curve shapes remain recognizable. Correlations that weight pressure and combustion-driven velocity respond earlier and more strongly near top dead center (TDC), for example Han's correlation. Correlations with stronger temperature moderation change more gradually and tend to peak later with broader profiles, for example the correlation of Bargende. With increasing load, some peaks broaden, but the expansion flank does not steepen markedly. On this basis, quantitative validation was undertaken to determine which correlation is most applicable under the studied conditions. Agreement with experiment was evaluated per load using the relative error, and overall accuracy was summarized by mean absolute percentage error (MAPE). Two additional criteria were applied: literature suitability for SI operation and a quality-versus-complexity assessment of required inputs and numerical robustness. Based on the stated evaluation criteria, the Han's correlation emerged as the most applicable for the present engine and operating window. Following the selection, Monte-Carlo sensitivity analysis was undertaken to assess the uncertainty of the heat-loss prediction and to rank the influence of the empirical constants. Monte-Carlo sampling of the Han empirical constants was carried out. The predicted heat-loss signal was found to be approximately normal with mild positive skew. Scatter plots showed an almost linear increase of the heat-loss signal with the primary scaling constant α_1 whereas k_{han1},k_{han2},k_{han3} and exhibited weak influence within the tested ranges. Accordingly, uncertainty is dominated by α_1. A reduction of the uncertainty in α_1 would be expected to yield the largest decrease in the spread of the heat-loss prediction, while tightening the remaining constants would have negligible effect. Taken together, the correlations were shown to reproduce the expected load trends, the Han formulation was identified as the most applicable within the present scope. The prediction uncertainty was found to be dominated by α_1. These findings provide a consistent basis for using Han in this engine and indicate that uncertainty-reduction efforts should prioritize α_1.

6.2. Recommendations

In light of the foregoing findings and acknowledged scope limits, targeted steps are proposed to strengthen the experimental basis and refine the modeling. Priority is placed first on measurements and validation scope, then on calibration of key constants, followed by model refinements informed by the new evidence, with reporting practices updated to include quantified uncertainty. Focused measurements should be performed to observe wall and gas thermal states directly. Fast surface-temperature sensors should be installed at in-cylinder boundary locations. Calibrations and measurement uncertainties should be documented and propagated into the model–experiment comparison. Broaden the validation matrix to additional loads, speeds, air-excess ratios (λ), and spark timings, and extend crank-angle coverage to include compression and expansion outside the start of combustion to end of combustion (SOC–EOC) window. This approach assesses the model under a wider range of thermal and fluid-dynamic conditions (higher and lower temperatures, varying flow intensities, earlier and later combustion) and permits the quantifies heat transfer during both pre-combustion and post-combustion periods. Together, these steps provide a stronger empirical basis to evaluate model behavior across operating regimes and to substantiate any subsequent improvements.

7

Bibliography

[1] Yunus A. Cengel and Michael A. Boles. *Thermodynamics: an Engineering Approach 8th Edition*. 2015.

[2] Christopher Depcik et al. “Determination of a heat transfer correlation for small internal combustion engines”. In: *Applied Thermal Engineering* 228 (June 2023), p. 120524. ISSN: 13594311. DOI: 10.1016/j.applthermaleng.2023.120524.

[3] Leonardo Fonseca et al. “Internal Combustion Engine Heat Transfer and Wall Temperature Modeling: An Overview”. In: *Archives of Computational Methods in Engineering* 27.5 (Nov. 2020), pp. 1661–1679. ISSN: 1134-3060. DOI: 10.1007/s11831-019-09361-9.

[4] Jerald A. Caton. *An Introduction to Thermodynamic Cycle Simulations for Internal Combustion Engines*. 2015. DOI: 10.1002/9781119037576.

[5] Lucca Henrion et al. “Characterization of radiative heat transfer in a spark-ignition engine through high-speed experiments and simulations”. In: *Oil & Gas Science and Technology – Revue d’IFP Energies nouvelles* 74 (July 2019), p. 61. ISSN: 1294-4475. DOI: 10.2516/ogst/2019030.

[6] Pablo Olmeda et al. “An adapted heat transfer model for engines with tumble motion”. In: *Applied Energy* 158 (Nov. 2015), pp. 190–202. ISSN: 03062619. DOI: 10.1016/j.apenergy.2015.08.051.

[7] Stijn Broekaert et al. “Heat transfer in premixed spark ignition engines part I: Identification of the factors influencing heat transfer”. In: *Energy* 116 (Dec. 2016), pp. 380–391. ISSN: 03605442. DOI: 10.1016/j.energy.2016.08.065.

[8] G.M. Kosmadakis, E.G. Pariotis, and C.D. Rakopoulos. “Heat transfer and crevice flow in a hydrogen-fueled spark-ignition engine: Effect on the engine performance and NO exhaust emissions”. In: *International Journal of Hydrogen Energy* 38.18 (June 2013), pp. 7477–7489. ISSN: 03603199. DOI: 10.1016/j.ijhydene.2013.03.129.

[9] Hai-Wen Ge et al. “Optimization of a HSDI Diesel Engine for Passenger Cars Using a Multi-Objective Genetic Algorithm and Multi-Dimensional Modeling”. In: *SAE International Journal of Engines* 2.1 (Apr. 2009), pp. 2009–01. ISSN: 1946-3944. DOI: 10.4271/2009-01-0715.

[10] Guillaume Bernard, Romain Lebas, and François-Xavier Demoulin. “A 0D Phenomenological Model Using Detailed Tabulated Chemistry Methods to Predict Diesel Combustion Heat Release and Pollutant Emissions”. In: Apr. 2011. DOI: 10.4271/2011-01-0847.

[11] E.G. Pariotis, G.M. Kosmadakis, and C.D. Rakopoulos. “Comparative analysis of three simulation models applied on a motored internal combustion engine”. In: *Energy Conversion and Management* 60 (Aug. 2012), pp. 45–55. ISSN: 01968904. DOI: 10.1016/j.enconman.2011.11.031.

[12] S. Verhelst and C.G.W. Sheppard. “Multi-zone thermodynamic modelling of spark-ignition engine combustion – An overview”. In: *Energy Conversion and Management* 50.5 (May 2009), pp. 1326–1335. ISSN: 01968904. DOI: 10.1016/j.enconman.2009.01.002.

[13] Yongrui Sun et al. “Development and validation of a marine sequential turbocharging diesel engine combustion model based on double Wiebe function and partial least squares method”. In: *Energy Conversion and Management* 151 (Nov. 2017), pp. 481–495. ISSN: 01968904. DOI: 10.1016/j.enconman.2017.08.085.

[14] Thomas De Cuyper et al. “Demonstrating the Use of Thin Film Gauges for Heat Flux Measurements in ICEs: Measurements on an Inlet Valve in Motored Operation”. In: Apr. 2016. DOI: 10.4271/2016-01-0641.

[15] D J Oude Nijeweme et al. “Unsteady in-cylinder heat transfer in a spark ignition engine: Experiments and modelling”. In: *Proceedings of the Institution of Mechanical Engineers, Part D: Journal of Automobile Engineering* 215.6 (June 2001), pp. 747–760. ISSN: 0954-4070. DOI: 10.1243/0954407011528329.

[16] Mika A Nuutinen et al. “Imbalance wall functions with density and material property variation effects applied to engine heat transfer computational fluid dynamics simulations”. In: *International Journal of Engine Research* 15.3 (Apr. 2014), pp. 307–324. ISSN: 1468-0874. DOI: 10.1177/1468087413481779.

[17] Stefano Fontanesi, Giuseppe Cicalese, and Matteo Giacopini. “Multiphase CFD-CHT Analysis and Optimization of the Cooling Jacket in a V6 Diesel Engine”. In: Oct. 2010. DOI: 10.4271/2010-01-2096.

[18] Stefano Fontanesi et al. “Integrated In-Cylinder/CHT Analysis for the Prediction of Abnormal Combustion Occurrence in Gasoline Engines”. In: Apr. 2014. DOI: 10.4271/2014-01-1151.

[19] S. Fontanesi et al. “Numerical investigation of the cavitation damage in the wet cylinder liner of a high performance motorbike engine”. In: *Engineering Failure Analysis* 44 (Sept. 2014), pp. 408–423. ISSN: 13506307. DOI: 10.1016/j.engfailanal.2014.05.025.

[20] Giuseppe Cicalese, Fabio Berni, and Stefano Fontanesi. “Integrated In-Cylinder / CHT Methodology for the Simulation of the Engine Thermal Field: An Application to High Performance Turbocharged DISI Engines”. In: *SAE International Journal of Engines* 9.1 (Apr. 2016), pp. 2016–01. ISSN: 1946-3944. DOI: 10.4271/2016-01-0578.

[21] Lei Zhang. “Parallel simulation of engine in-cylinder processes with conjugate heat transfer modeling”. In: *Applied Thermal Engineering* 142 (Sept. 2018), pp. 232–240. ISSN: 13594311. DOI: 10.1016/j.applthermaleng.2018.06.084.

[22] Denys STEPANENKO and Zbigniew KNEBA. “Thermodynamic modeling of combustion process of the internal combustion engines – an overview”. In: *Combustion Engines* 178.3 (July 2019), pp. 27–37. ISSN: 2300-9896. DOI: 10.19206/CE-2019-306.

[23] H. K. Rashedul et al. “Numerical study on convective heat transfer of a spark ignition engine fueled with bioethanol”. In: *International Communications in Heat and Mass Transfer* 58 (Nov. 2014), pp. 33–39. ISSN: 0735-1933. DOI: 10.1016/J.ICHEATMASSTRANSFER.2014.08.019.

[24] Amel Djouadi and Fatiha Bentahar. “Combustion study of a spark-ignition engine from pressure cycles”. In: *Energy* 101 (Apr. 2016), pp. 211–217. ISSN: 03605442. DOI: 10.1016/j.energy.2016.02.013.

[25] Junseok Chang et al. “New Heat Transfer Correlation for an HCCI Engine Derived from Measurements of Instantaneous Surface Heat Flux”. In: Oct. 2004. DOI: 10.4271/2004-01-2996.

[26] Sary Awad et al. “Single zone combustion modeling of biodiesel from wastes in diesel engine”. In: *Fuel* 106 (Apr. 2013), pp. 558–568. ISSN: 00162361. DOI: 10.1016/j.fuel.2012.11.051.

[27] Anand M Shivapuji and S Dasappa. “Experiments and zero D modeling studies using specific Wiebe coefficients for producer gas as fuel in spark-ignited engines”. In: *Proceedings of the Institution of Mechanical Engineers, Part C: Journal of Mechanical Engineering Science* 227.3 (Mar. 2013), pp. 504–519. ISSN: 0954-4062. DOI: 10.1177/0954406212463846.

[28] J. Galindo et al. “Correlations for Wiebe function parameters for combustion simulation in two-stroke small engines”. In: *Applied Thermal Engineering* 31.6-7 (May 2011), pp. 1190–1199. ISSN: 13594311. DOI: 10.1016/j.applthermaleng.2010.12.020.

[29] Melih Yıldız and Bilge Albayrak Çeper. “Zero-dimensional single zone engine modeling of an SI engine fuelled with methane and methane-hydrogen blend using single and double Wiebe Function: A comparative study”. In: *International Journal of Hydrogen Energy* 42.40 (Oct. 2017), pp. 25756–25765. ISSN: 03603199. DOI: 10.1016/j.ijhydene.2017.07.016.

[30] Morteza Fathi et al. “Stand-alone single- and multi-zone modeling of direct injection homogeneous charge compression ignition (DI-HCCI) combustion engines”. In: *Applied Thermal Engineering* 125 (Oct. 2017), pp. 1181–1190. ISSN: 13594311. DOI: 10.1016/j.applthermaleng.2017.07.123.

[31] Mohand Said Lounici et al. “Investigation on heat transfer evaluation for a more efficient two-zone combustion model in the case of natural gas SI engines”. In: *Applied Thermal Engineering* 31.2-3 (Feb. 2011), pp. 319–328. ISSN: 1359-4311. DOI: 10.1016/J.APPLTHERMALENG.2010.09.012.

[32] Yann G. Guezennec and Wajdi Hamama. “Two-Zone Heat Release Analysis of Combustion Data and Calibration of Heat Transfer Correlation in an I. C. Engine”. In: Mar. 1999. DOI: 10.4271/1999-01-0218.

[33] Allan T. Kirkpatrick. *Internal Combustion Engines*. Wiley, Nov. 2020. ISBN: 9781119454502. DOI: 10.1002/9781119454564.

[34] Gary Borman and Kazuie Nishiwaki. “Internal-combustion engine heat transfer”. In: *Progress in Energy and Combustion Science* 13.1 (Jan. 1987), pp. 1–46. ISSN: 03601285. DOI: 10.1016/0360-1285(87)90005-0.

[35] J.L.S. Fagundez et al. “Comparative analysis of different heat transfer correlations in a two-zone combustion model applied on a SI engine fueled with wet ethanol”. In: *Applied Thermal Engineering* 115 (Mar. 2017), pp. 22–32. ISSN: 13594311. DOI: 10.1016/j.applthermaleng.2016.12.121.

[36] Eichelberg. “Some New Investigations on Old Combustion-Engine Problems. I-V”. In: *Engineering* 148 (1939).

[37] Eric Ollivier et al. “Detection of knock occurrence in a gas SI engine from a heat transfer analysis”. In: *Energy Conversion and Management* 47.7-8 (May 2006), pp. 879–893. ISSN: 01968904. DOI: 10.1016/j.enconman.2005.06.019.

[38] G. Woschni. “A Universally Applicable Equation for the Instantaneous Heat Transfer Coefficient in the Internal Combustion Engine”. In: Feb. 1967. DOI: 10.4271/670931.

[39] W. J. D. Annand. “Heat Transfer in the Cylinders of Reciprocating Internal Combustion Engines”. In: *Proceedings of the Institution of Mechanical Engineers* 177.1 (June 1963), pp. 973–996. ISSN: 0020-3483. DOI: 10.1243/PIME{_}PROC{_}1963{_}177{_}069{_}02.

[40] G. Sitkei and G. V. Ramanaiah. “A Rational Approach for Calculation of Heat Transfer in Diesel Engines”. In: Feb. 1972. DOI: 10.4271/720027.

[41] Sung Bin Han et al. “Empirical Formula for Instantaneous Heat Transfer Coefficient in Spark Ignition Engine”. In: Oct. 1997. DOI: 10.4271/972995.

[42] Michael Bargende. “Ein allgemeingültiger Wärmeübergangskoeffizient für die Zylinderinnenwand von Ottomotoren”. PhD thesis. Stuttgart: Universität Stuttgart, 1991.

[43] John B. Heywood. *Internal Combustion Engine Fundamentals*. 1st. New York: McGraw-Hill, 1988.

[44] Konstantinos I. Kiouranakis et al. “Heat release behavior in a natural gas lean-burn SI marine engine: Exploring the impact of bowl-in and squish combustion on performance and emissions”. In: *Applied Thermal Engineering* 279 (Nov. 2025), p. 127509. ISSN: 13594311. DOI: 10.1016/j.applthermaleng.2025.127509.

[45] Günter F. Hohenberg. “Advanced Approaches for Heat Transfer Calculations”. In: Feb. 1979. DOI: 10.4271/790825.